



## Tracing CO<sub>2</sub> and helium origins of mineral spring water of the Water Circuit of Minas Gerais in southeastern Brazil

Hendryk Gemeiner <sup>a,b</sup>, Hung Kiang Chang <sup>a,b,\*</sup>, Larissa Neris Alcara <sup>a</sup>, Marcelo Martins Reis <sup>a</sup>, Peter H. Barry <sup>c</sup>, Amauri Antonio Menegário <sup>b</sup>

<sup>a</sup> Basin Studies Laboratory (IGCE-LEBAC), São Paulo State University (UNESP), Avenida 24-A, 1515, Rio Claro, SP 13506-900, Brazil

<sup>b</sup> Environmental Studies Center (CEA), São Paulo State University (UNESP), Avenida 24-A, 1515, Rio Claro, SP 13506-900, Brazil

<sup>c</sup> Marine Chemistry and Geochemistry Department, Woods Hole Oceanographic Institution, Woods Hole, MA, USA

### ARTICLE INFO

Editor: Dr. Don Porcelli

**Keywords:**

CO<sub>2</sub> springs  
Noble gases  
Helium isotopes  
Brasilia Belt

### ABSTRACT

The Water Circuit of Minas Gerais, situated in the southeastern region of the Brazilian state of Minas Gerais, has garnered significant interest since the 19th century due to the abundance of mineral springs with heightened mineral compositions and high levels of CO<sub>2</sub>. However, despite decades of research, the origins of this natural CO<sub>2</sub> enrichment phenomenon in these springs remain unclear. Here, we present the first noble gas isotope data from these spring waters combined with hydrochemical data. Calcium bicarbonate waters predominate in the spa town parks of Caxambu, Águas de Contendas and Lambari, whereas sodium bicarbonate and "mixed type" is found in the Cambuquira park. All samples display high He concentrations and elevated <sup>4</sup>He/<sup>20</sup>Ne values with respect to atmospheric values, indicating a deep origin and the gradual accumulation of radiogenic <sup>4</sup>He in the waters. Spring samples show air-corrected <sup>3</sup>He/<sup>4</sup>He (R<sub>c</sub>/R<sub>a</sub>) values between 0.55 and 3.39 R<sub>a</sub>, suggesting an admixture of crustal and mantle volatile contributions. A consistent <sup>3</sup>He/<sup>4</sup>He decrease with increasing distance from the Caxambu shear zone is observed, indicating that the release of deep fluids is fault controlled. We suggest that major fault segments within the Caxambu shear zone serve as continuous pathways for the ascent of mantle-derived CO<sub>2</sub> and He, enriching the springs of the Water Circuit region. Carbon isotope data indicates a significant contribution of carbonate-derived CO<sub>2</sub>. We combined discharge estimates with carbon concentrations to quantify a CO<sub>2</sub> flux of 4.26 × 10<sup>6</sup> mol year<sup>-1</sup> into the surface system from all springs in the four spa parks.

### 1. Introduction

Source determination of elevated CO<sub>2</sub> concentrations in natural waters, coupled with an understanding of CO<sub>2</sub> migration mechanisms within the subsurface, is critical for understanding the fundamental principles that underpin carbon capture and storage (CCS) initiatives. In this context, the use of noble gases (NG) to fingerprint natural CO<sub>2</sub> pathways, from the source to the surface, in different geological settings has been extensively studied in recent years (Gilfillan et al., 2008; Gilfillan et al., 2011; LaForce et al., 2014; Karolyte et al., 2019; Ju et al., 2020; Györe et al., 2021; Zappone et al., 2021; Barry et al., 2013, 2019, 2022, 2025). The excellent tracer properties of noble gases are due to their chemical inertness and their distinct elemental and isotopic composition in the subsurface, which are derived from three distinct natural sources: (1) dissolved atmospheric noble gases (<sup>20</sup>Ne, <sup>36</sup>Ar) in meteoric water entering the subsurface during recharge, (2) radiogenic

sources within the crust, whereby noble gases like <sup>4</sup>He and <sup>40</sup>Ar are produced by radioactive decay of U, Th and K, and (3) terrigenic sources, where mantle derived elements (e.g., <sup>3</sup>He trapped in the mantle during accretion of Earth) are constantly degassing from the mantle to the crust and surface (Marty and Jambon, 1987; Marty and Tolstikhin, 1998; Marty and Zimmermann, 1999; Ballentine and Burnard, 2002; Gilfillan et al., 2011; Aeschbach-Hertig and Solomon, 2013).

One of the most direct methods for studying CO<sub>2</sub> migration in the subsurface involves the analysis of NGs in heavily carbonated water obtained from springs and groundwater wells. For example, NG data from spring and groundwater wells were compared with NG data from deep natural CO<sub>2</sub> reservoirs to trace CO<sub>2</sub> along fault zones at the St. Johns Dome (USA) (Gilfillan et al., 2011) and in Erzin-Hatay (Turkey) (Yasin and Yüce, 2023). Noble gas and stable isotope data from gas fields and mineral spring waters indicated mantle-sourced CO<sub>2</sub> in the Otway Basin, Central Victorian Highlands (Karolyte et al., 2019) and Great

\* Corresponding author.

E-mail address: [chang.hung-kiang@unesp.br](mailto:chang.hung-kiang@unesp.br) (H.K. Chang).

Artesian Basin (Italiano et al., 2014; Ring et al., 2016) of Australia. The combination of measurements of  $\delta^{13}\text{C}$  of  $\text{CO}_2$ ,  $\text{CO}_2$  and He concentrations, along with the analysis of Ne and Ar isotopes from gas samples of  $\text{CO}_2$  seeps from riverine and groundwater samples confirmed plume-related mantle degassing beneath Southern Africa (Gilfillan et al., 2019). Helium isotope data ( ${}^3\text{He}/{}^4\text{He}$ ) from geothermal springs in the Colorado Rocky Mountains provided evidence for mantle derived  $\text{CO}_2$  degassing in groundwater (Karlstrom et al., 2013).

The *Water Circuit of Minas Gerais* (*Círculo das Águas de Minas Gerais*) is a region in the south of the Brazilian state of Minas Gerais which hosts several mineral water springs located in the towns of Águas de Contendas, Cambuquira, Caxambu, Conceição do Rio Verde, Lambari and São Lourenço. Beginning in the 19th century, spa parks were installed in these towns to explore these springs for commercial mineral water production and therapeutic baths, representing a great economic and touristic importance for the region up until this day. These waters are characterized by their relatively high content of Ca, Mg, K, Na, Fe and S, and mostly by their remarkably high content of dissolved  $\text{CO}_2$  (CODEMGE, 2018). However, the source of this natural  $\text{CO}_2$  enrichment has remained unclear. High contents of dissolved  $\text{CO}_2$  in natural mineral waters can originate from various sources, such as magmatic degassing, deep-seated mantle degassing, metamorphic devolatilization, the oxidative breakdown of organic substances, and the interaction between water and sedimentary carbonates (Marques et al., 2000; Cartwright et al., 2002). The existence of mantle-derived carbon, or carbon sourced from magma, can indicate the presence of contemporary or recent volcanic events that might not be observable through surface geological features (Cartwright et al., 2002).

In order to update and deepen the geological, geophysical, hydrogeological, hydrogeochemical and hydro-isotopic knowledge on the mineral waters of the Water of Circuit of Minas Gerais, as well as to achieve a better understanding of the origin of these mineral waters, the Agency for Development of the State of Minas Gerais (CODEMGE – Companhia de Desenvolvimento de Minas Gerais) started a joint project with researchers from several different institutions and universities, generating a vast data bank published in 2018 (CODEMGE, 2018). With the obtained data, the authors classified the mineral waters as meteoric paleowaters that became deep-circulating groundwater. The generated conceptual hydrogeological models portray deep underground and supra-basinal circulation systems, with calculated geotemperatures of up to 135 °C and circulation depths of up to 5639 m. The dating of mineral waters with the  ${}^{14}\text{C}$  method revealed ages that exceeded 43,500 years with the majority being above 25,000 years, showing low percentages of modern carbon and slightly negative  ${}^{13}\text{C}$  values, which are indicative of inorganic carbon. The mineral waters do not show chemical-isotopic relationships or evidence of a direct physical connection with groundwater from shallower aquifers (alluvium layers and weathered mantle rocks). Finally, the authors concluded that the mineral waters of the Water Circuit originated from rainwater that infiltrated the northern slope of the Serra da Mantiqueira thousands of years ago. It was proposed that during its prolonged subsurface transit, the water percolated through fractures in high-grade metamorphic rocks, triggering the release of  $\text{CO}_2$  from fluid inclusions and chemical reactions involving carbon compounds within the mineral structures of these rocks, such as the dissolution of carbonates (CODEMGE, 2018). However, approximately 300 km from the Water Circuit, helium isotope analysis revealed that the high  $\text{CO}_2$  concentrations in offshore hydrocarbon reservoirs of the Santos Basin have a significant mantle-derived influence (Ferraz et al., 2019). A hypothesis to explain this observation is the extreme thinning of the continental crust on the São Paulo Plateau, the distal portion of the Santos Basin, which may have allowed mantle-derived materials to ascend to upper crustal levels (Ferraz et al., 2019; Gamboa et al., 2019). Fault systems linked to these magmatic intrusions can channel  $\text{CO}_2$  into the upper sedimentary layers, directing it towards the surface (Ferraz et al., 2019).

In this context, the present work represents the first study using NG

data to draw inferences on the origin of  $\text{CO}_2$  and He in spring waters from the Water Circuit of Minas Gerais. Besides NG and  $\text{CO}_2$  concentrations and chemical water composition,  ${}^3\text{He}/{}^4\text{He}$  and  ${}^{40}\text{Ar}/{}^{36}\text{Ar}$  values were determined to discern contributions from deep-seated volatile sources versus those from crustal carbonates. Moreover, these findings could provide valuable insights into local and regional hydrogeology.

## 2. Study site and geological setting

The  $\text{CO}_2$  enriched spring waters from the Water Circuit in Minas Gerais represent a remarkable hydrogeological phenomenon within the stable tectonic framework of eastern South America. The eastern part of South America, largely represented by the South American Platform, records a complex tectonic history that dates back to the Paleoproterozoic, culminating in the formation of the Gondwana supercontinent during the Neoproterozoic until the Cambrian (Meert and Van Der Voo, 1997). The region is dominated by cratonic blocks, such as the São Francisco Craton, which is surrounded by Neoproterozoic orogenic belts formed during the Brasiliano orogenic cycle, including the Brasília, Ribeira, Araçuaí, and Dom Feliciano belts. The shear zones that today mark southeastern Minas Gerais - including Três Corações, Jesuânia, Freitas, and Caxambu - were formed or reactivated in this context of continental collision at the end of the Neoproterozoic. With the end of the Brasiliano orogeny and the stabilization of the platform in the early Paleozoic, the eastern part of South America began to act as a rigid basement for large intracratonic sedimentary basins, such as the Paraná Basin. However, despite the apparent stability since then, many of these shear zones preserve deep lithospheric connectivity (Cordani et al., 2016).

The region of the Water Circuit of Minas Gerais occupies a part of the Serra da Mantiqueira mountains, drained by the river Rio Verde and its tributaries Lambari and Baependi in the south of Minas Gerais (CODEMGE, 2018). The relief of this region is characterized by a set of mountains and ridges oriented preferably in the NE-SW direction with maximum altitude of 1600 m, and the Rio Verde depression, consisting of large valleys oriented in the NE-SW, NS and NW-SE directions (CODEMGE, 2018). All four spa town parks that were sampled are located in the Rio Verde depression (Beato et al., 1998). Trouw et al. (1994) concluded that the Water Circuit of Minas Gerais is situated in an interference zone between two Brazilian orogenic systems: the Southern Brasília Belt and the Ribeira Belt. The primary configuration of the Southern Brasília Belt comprises a zone of folding and thrusting involving Neoproterozoic metasedimentary rocks, overlain by a system of sub-horizontal spoon-shaped morphology of metamorphic nappes transported to the southeast and east directions (Valeriano et al., 2004; Valeriano et al., 2008; Valeriano, 2017). This belt extends more than 1200 km along the western margin of the São Francisco Craton (Valeriano, 2017) and its genesis, between 650 and 630 Ma ago, is interpreted as a product of the convergence between the passive margin of the São-Francisco paleocontinent to the east and the active margin of Paranapanema block to the west (Mantovani et al., 2005). It encompasses an Archean/Paleoproterozoic basement, along with Meso/Neoproterozoic supracrustal assemblages accumulated in rift basins, passive margins, and foreland basins (Valeriano et al., 2004; Valeriano et al., 2008; Valeriano, 2017). On the other side, the Ribeira Belt is described as a polyphasic orogenic belt characterized by an association of northwesterly faults and folds, which alternate with large northeasterly dextral shear zones. This belt delineates the central sector of the Mantiqueira Orogenic System, situated to the south-southeast (S-SE) of the São Francisco craton. It spans approximately 1500 km along the southeastern Brazilian Atlantic margin, as outlined by Corrales (2019). The belt results from a southeast to northwest (SE-NW) convergence and stacking system involving the São Francisco, Congo, and Paranapanema cratons, as well as various tectonic terrains such as tonalitic, gabbroic and dioritic magmatic arcs and microplates, during the consolidation of the Western Gondwana continent (Almeida et al., 1973; Cordani, 1973;

Alita, 2017). Part of its framework is the Archean/Paleoproterozoic basement and Mesoproterozoic sedimentary and volcano-sedimentary successions, assemblages of Neoproterozoic magmatic arcs and a Neoproterozoic passive margin sedimentary pile (Almeida et al., 1981; Campos Neto and Caby, 2000; Trouw et al., 2000; Trouw et al., 2013; Heilbron et al., 2008; Heilbron et al., 2017; CODEMGE, 2018). As part of the outer portion of the Southern Brasília Belt that received tectonic influence from the Ribeira Belt, the Water Circuit region exposes gneissic rocks from the Archean/Paleoproterozoic substrate and meta-sedimentary rocks (schists, gneisses and quartzites) of the Andrelândia Megasequence from the Neoproterozoic (Fig. 1). These units occur in the region as a stack of five nappes, which are allochthonous (Ebert, 1971; Paciullo et al., 2000; Ribeiro et al., 2013; CODEMGE, 2018) and have been intruded by Neoproterozoic leucogranites, as well as diabase dykes and alkaline rocks of undetermined Phanerozoic ages (CODEMGE, 2018).

The Caxambu spa park has eleven mineral springs and is located at an altitude of 958 m a.s.l. It belongs to the geological group of the Andrelândia – São Vicente Complex. In this context, the predominant lithological makeup consists of biotite-orthogneiss, thin-banded biotite-paragneiss, schists associated with quartzites and granitic leucogneiss, cut by alkaline gap dykes and mafic dykes. The mineral springs in the Caxambu water park stem from the presence of fractured hydrogeological domains within its subterranean hydrological system (Beato et al., 1998; CODEMGE, 2018; Damatto, 2021).

The Águas de Contendas spa park has four mineral water springs and is situated at an altitude of 873 m a.s.l. The area is part of the Barbacena – Lambari geological complex, distinguished primarily by its igneous rock compositions, as well as quartzites and schists found in the nested valleys (Costa, 1996). The lithological assemblage comprises biotite-gneiss, interspersed with amphibolytic granules. On a smaller scale, the basement is intersected by small bodies of leucogranite, along with a weathered alkaline dike (CODEMGE, 2018). The hydrological system is

part of the Contendas riverine sub-basin and includes both porous granular and fractured aquifers. The former consists of alluvial sediments along the Bengo stream and alteration layers that cover the bedrock. The fractured type is found in crystalline rocks, from which the mineral water springs originate (Beato et al., 1998; CODEMGE, 2018; Damatto, 2021).

The Lambari spa park consists of seven mineral water springs and is located in the center of the town at an altitude of 887 m a.s.l. Geologically, the region belongs to the Barbacena – Lambari Complex characterized by a lithology of fine-grained biotite gneiss interspersed with amphibolytic biotite gneiss, biotite-granada gneiss, and amphibolytic dioritic gneiss, as well as occurrences of leucogranite intrusions (Beato et al., 1998; CODEMGE, 2018; Meneghini et al., 2019; Damatto, 2021).

The five mineral water springs in the Cambuquira spa park (located at an altitude of 950 m) belong geologically to the Andrelândia – Lambari Complex. The park is situated within a geological formation primarily consisting of garnetiferous schists with gneiss intercalations, both saprolitized with a small part of associated quartzite (Beato et al., 1998; Santos and Damatto, 2017; Damatto, 2021).

### 3. Methods

#### 3.1. Sampling campaign

In total, 21 springs/ wells and one creek were sampled for physicochemical analysis in the spa town parks Águas de Contendas, Cambuquira, Caxambu and Lambari in June/July of 2023. At each park, gas samples were taken from one spring/well, except for Caxambu, where three springs were sampled. Additionally, in November 2023, a second sampling campaign was conducted, obtaining gas samples from one spring/well at each location, except for Caxambu, where two springs were sampled. During this campaign, water samples in copper tubes were taken for  $^3\text{He}/^4\text{He}$  analysis from one spring/well at each park.

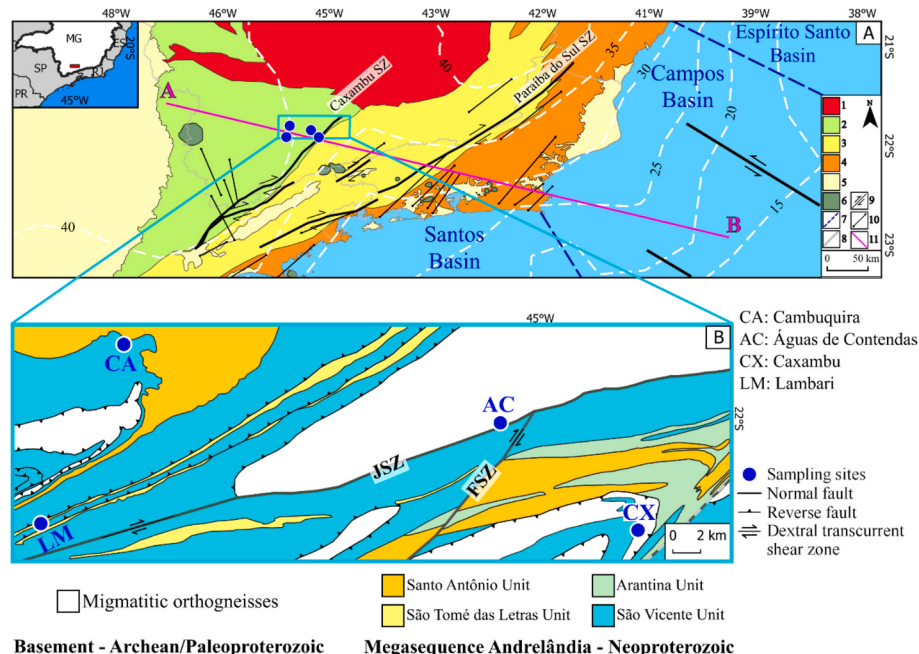


**Fig. 1.** A) Simplified tectonic map of Southeastern Brazil based on Heilbron et al. (1995), Campos Neto and Figueiredo (1995) in Heilbron et al. (2000). The tectonic features were extracted from Meisling et al. (2001), Almeida et al. (2013) and Trouw et al. (2013). Legend: 1 - São Francisco craton; 2 - Brasília Belt; 3 - Ribeira Belt (Occidental Terrane); 4 - Ribeira Belt (Oriental Terrane); 5 - Paraná basin; 6 - Meso-Cenozoic Alkaline rocks; 7 - Boundary of sedimentary basins; 8 - Crustal thickness (km) extracted from Assumpção et al. (2013); 9 - Shear zones (SZ); 10 - Largest dikes; 11 - Cross-section Line. B) Geologic map of the region of the Water Circuit of Minas Gerais featuring sampling sites (blue points). Shear zones Jesuânia (SJZ) and Freitas (SZF). Geological formations include the basement (migmatitic orthogneisses) and the Andrelândia Megasequence consisting of the Santo Antônio (biotite schist/gneiss), São Tomé das Letras (quartzites), Arantina (thick biotite schist/gneiss), and São Vicente (biotite paragneiss) units. Map was generated based on geological maps in CODEMGE (2018). (For interpretation of the references to colour in this figure legend, the reader is referred to the web version of this article.)

Characteristics of all sampling sites are detailed in the Supplementary Material in Table S1.

### 3.2. Physicochemical analysis

Physicochemical parameters (water temperature, electrical conductivity, pH, redox potential, total dissolved solids and salinity) of the spring waters were directly measured in the field using a HI9828/10-1 multiparameter water quality meter (Hanna Instruments) and a multi-function water quality tester. Furthermore, content of dissolved CO<sub>2</sub> and O<sub>2</sub> of the waters was determined also in the field using a CboxQC At-line measuring instrument (Anton Paar).

Water samples were collected in plastic bottles and taken refrigerated directly to the laboratory where they were passed through 0.45 µm membrane inline filters. Subsequently, the alkalinity was determined by potentiometric titration (Model 888 Titrando, Metrohm). The major anions and cations in the samples were determined using ionic chromatography (Compact IC761, Metrohm), while metals were determined using inductively coupled plasma optical emission spectroscopy (ICP OES model 5800, Agilent).

### 3.3. Analysis of dissolved gas concentrations

Gas samples for total dissolved gas concentrations were taken with a self-made extraction device consisting of a water and gas flow line separated by a membrane contactor (MM-1.7 × 8.75 Series, 3 M™ Liqui-Cel™) (as described in Gemeiner et al., 2025). In summary, a water flow is applied through the lumen side of the membrane and a small diaphragm pump is connected to the ends of the shell side of the membrane generating a vacuum. As a result, gas is extracted from the water passing through the membrane and is directed through gas tight connections to a sample multi-foil bag of a volume of 0.5 L, where the sample gas was accumulated until about 80 % of the bags total volume capacity.

The bags were analyzed for Ar, CO<sub>2</sub>, N<sub>2</sub> and O<sub>2</sub> by the gas quadrupole mass spectrometer Omnistar GSD 350 (Pfeiffer Vacuum). The sample bags were directly connected with the capillary of the Omnistar by penetrating the capillary needle through the septum of the polypropylene fitting of the bag. The Faraday cup detector of the instrument was used to quantify CO<sub>2</sub>, N<sub>2</sub> and O<sub>2</sub>, whereas the Secondary Electron Multiplier was used for the quantification of Ar. Dwell times were 256 ms for N<sub>2</sub> and O<sub>2</sub>, 512 ms for CO<sub>2</sub> and 4096 ms for Ar. Time of analysis was 5 min for each sample and individual analyte. To obtain absolute concentration values, detector signals of the sample measurements were directly compared to signals from calibration measurements of a reference gas with an air-like composition.

### 3.4. Calculation of absolute dissolved gas concentrations

Using gas molar fractions measured in the sample bags, the dissolved concentrations of the respective components in 1 g of spring water (C<sub>i</sub><sup>w</sup> in cm<sup>3</sup>STP g<sup>-1</sup>) can be deduced by applying Henry's Law, described by Eq. 1 shown in Kipfer et al. (2002):

$$C_i^w = C_i^g / H_i(T, S) \quad (1)$$

where C<sub>i</sub><sup>g</sup> is the partial pressure of the respective gas inside the sample bag and H<sub>i</sub> (atm/(cm<sup>3</sup>STP g<sup>-1</sup>)) is the Henry coefficient. Since atmospheric pressure is assumed inside the sampling bags, C<sub>i</sub><sup>g</sup> is calculated by multiplying the atmospheric pressure by the measured volume fraction (%) of gas i.

The Henry coefficient depends on the temperature (T) and salinity (S) of the sampled water, calculated from the solubility data given by Weiss (1974) for CO<sub>2</sub> and Weiss (1970) for Ar, N<sub>2</sub> and O<sub>2</sub>. The reported solubility values given as aquatic concentration of gas i at equilibrium (C<sub>i</sub><sup>\*</sup>) for the respective temperature and salinity in ml kg<sup>-1</sup> were converted in mol cm<sup>-3</sup> and Eq. 2 was used to calculate the respective Henry

coefficient (H<sub>i</sub>):

$$H_i(T, S) = P_i / C_i^*(T, S) \quad (2)$$

where P<sub>i</sub> represents the known partial pressure of gas i in the atmosphere.

### 3.5. Analysis of NG isotopes

Water samples for noble gas analysis were collected in copper tubes according to the sampling protocol provided in Aeschbach-Hertig and Solomon (2013) and Barry et al. (2022). The sampling setup consisted of a copper tube which was fixed between stainless clamps on both ends of the tube screwed on an aluminum rack. The tube was connected to the outlet of the well with a plastic hose and flushed for several minutes, until parameters (i.e., electrical conductivity, temperature, pH and dissolved oxygen) showed stable values. We ensured that no bubbles remained in the system by squeezing the hoses and gently tapping on the tube and clamps. Once the system was well rinsed, the clamp on the end of the tube was closed by cold welding followed by the clamp on the inlet, providing a sealed and leak tight water sample. Samples were then shipped and analyzed at the Barry Lab of the Woods Hole Oceanographic Institution (Massachusetts, USA) using a Nu Noblesse HR mass spectrometer interfaced to a noble gas processing and purification inlet system performing full cryogenic separation and purification of the noble gases prior to inlet into the mass spectrometer (Bekaert et al., 2023).

## 4. Results and discussion

### 4.1. Chemical composition of spring waters

The measured physicochemical parameters of water samples are listed in Table S2 in the Supplementary Material. The chemical data were used to generate a Piper diagram (Fig. 2) for classifying and comparing the waters from the four different parks. Calcium bicarbonate waters predominate in Caxambu, Águas de Contendas and Lambari, whereas sodium bicarbonate and mixed type was found in Cambuquira. These results are in agreement with the results reported in CODEMGE (2018).

In-situ measured parameters of salinity, water temperature, dissolved CO<sub>2</sub> and O<sub>2</sub> concentrations of sampled spring and well waters are shown in Table S3. Salinity ranged from 277 mg kg<sup>-1</sup> at the Dom Pedro Spring in Caxambu (CX-DP) to 24 mg kg<sup>-1</sup> at the Roxo Rodrigues spring in Cambuquira (CA-RR). A seasonal difference in salinity was observed in Mayrink II spring in Caxambu (CX-M2), where salinity was slightly higher in June versus in November. Water temperatures also displayed seasonal variability, with values in November (23.3 °C to 26.1 °C) exceeding those in June/July (19.2 °C to 24.9 °C), on average. Mayrink II spring in Caxambu (CX-M2) consistently exhibited the highest water temperatures in both seasons. The CO<sub>2</sub> and O<sub>2</sub> concentrations determined using the analytical methods described in Section 3.3 differed on average by 25 % and 38.3 %, respectively, from the measured concentrations with the CBox QC device. This difference is due to the higher precision associated with the mass spectrometer analysis vs the CBox QC. The CBox QC determines the CO<sub>2</sub> concentration by using a multiple volume expansion method, whereas the CO<sub>2</sub> content is measured at two different volume expansions in a calibrated chamber. The O<sub>2</sub> concentration is determined via optochemical oxygen measurement using a sensor with an oxygen-sensitive layer consisting of luminescent dye embedded in a gas-permeable polymeric matrix, which is in direct contact with the sample. Neither of the two methods can match the precision offered by mass spectrometry. Consequently, we exclusively used the results obtained through mass spectrometry for the subsequent data evaluation. However, in situ results obtained from the CBox QC proved highly valuable in offering a real-time overview of the

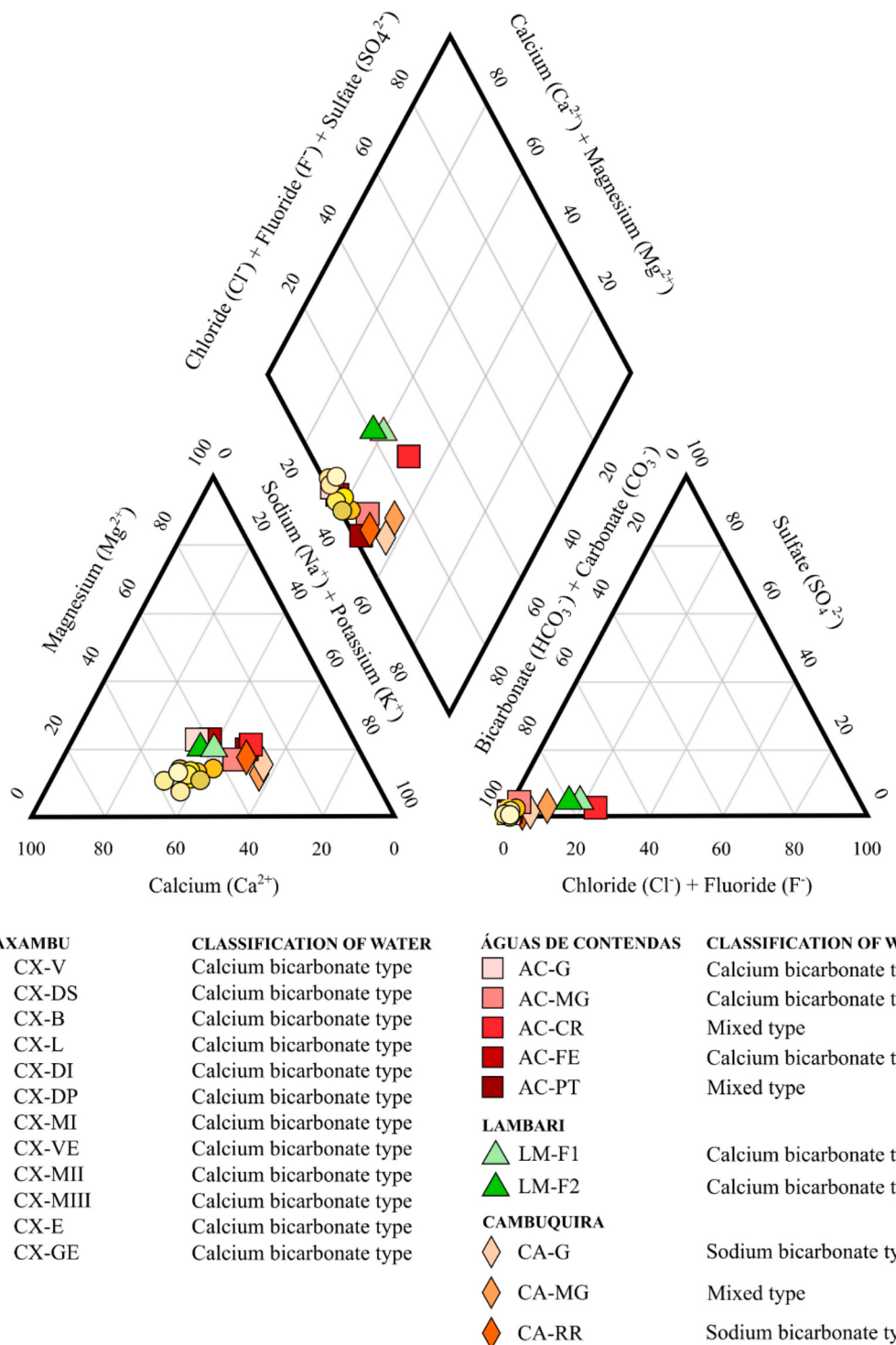


Fig. 2. Piper diagram including results of anions and cations of all sampling points.

anticipated CO<sub>2</sub> and O<sub>2</sub> concentrations in the spring waters. Dissolved CO<sub>2</sub> concentrations were notably elevated in Águas de Contendas in both seasons compared to the other water parks, reaching up to 1478 mg L<sup>-1</sup> at the well AC-PT in November. Conversely, the Mayrink III spring in Caxambu (CX-M3) recorded the lowest CO<sub>2</sub> concentrations at 383 mg L<sup>-1</sup> of all measured springs. A distinct rise in CO<sub>2</sub> concentrations in November compared to June/July was observed for all measured springs and wells. Measured dissolved oxygen concentrations are in good agreement between June/July and November at all sampling localities, ranging between 0.6 mg L<sup>-1</sup> (AC-PT) and 2.6 mg L<sup>-1</sup> (CA-RR).

Based on hydrochemical data, saturation indices were calculated using PHREEQC Interactive software (version 3.8.6.17100) for clay minerals (i.e., illite and Ca-montmorillonite), and for minerals such as calcite, aragonite, and quartz whose formation is related to rock weathering processes and silicate hydrolysis. Furthermore, manual optimization was performed in the software by adjusting the log(pCO<sub>2</sub>) value in the EQUILIBRIUM\_PHASES command until the simulated pH values matched those observed in the field analyses, thus allowing the estimation of CO<sub>2</sub> partial pressure (pCO<sub>2</sub>) in equilibrium with the solution (Table 1). Most spring waters were undersaturated with respect to

**Table 1**Saturation indices of minerals and pCO<sub>2</sub> levels in spring water samples based on hydrochemical data.

Sample ID	Aragonite	Ca-Montmorillonite	Calcite	Dolomite	Illite	Quartz	p(CO <sub>2</sub> ) [atm]
AC-CR	-3.85	1.93	-3.71	-7.44	0.08	-0.18	0.01
AC-FE	-3.31	1.41	-3.17	-6.47	-1.05	0.68	0.34
AC-G	-2.25	3.34	-2.10	-4.37	1.32	0.79	0.39
AC-MG	-4.43	1.06	-4.29	-8.79	-1.39	0.51	0.03
AC-PT	-3.40	1.81	-3.25	-6.60	-0.65	0.68	0.35
CA-G	-3.02	2.97	-2.88	-5.93	1.41	0.06	0.35
CA-MG	-5.39	-3.18	-5.24	-10.72	-6.48	-0.09	0.30
CA-RR	-5.18	-1.59	-5.03	-10.19	-4.67	0.20	0.23
CX-B	-0.82	5.65	0.62	0.65	5.06	0.55	0.27
CX-DI	-2.63	4.46	-0.16	-0.80	3.54	0.57	0.35
CX-DP	-2.05	0.70	-1.91	-4.33	-1.01	0.20	0.31
CX-DS	0.45	5.68	0.60	0.47	5.24	0.39	0.31
CX-E	0.01	4.58	0.15	-0.19	3.82	0.53	0.32
CX-GE	0.63	5.99	0.78	1.08	5.65	0.51	0.10
CX-L	-1.15	3.16	-1.00	-2.51	1.86	0.43	0.32
CX-M1	-2.75	0.13	-2.61	-5.69	-1.90	0.12	0.30
CX-M2	-2.69	-0.17	-2.54	-5.53	-2.10	0.13	0.24
CX-M3	-3.87	-0.52	-3.73	-7.84	-2.79	-0.02	0.06
CX-V	-2.48	0.25	-2.34	-5.17	-1.78	0.14	0.33
CX-VE	0.05	5.02	0.19	-0.11	4.28	0.48	0.32
LM-F1	-4.23	-1.71	-4.08	-8.31	-4.45	0.00	0.35
LM-F2	-4.31	-2.13	-4.17	-8.49	-4.92	0.01	0.42

calcite, aragonite, and dolomite, indicating active carbonate dissolution. Springs from the Caxambu spa park generally exhibit higher saturation indices for calcite, dolomite, and illite, suggesting more mineralized water, possibly resulting from deeper flow paths or prolonged water–rock interaction. Furthermore, samples from Caxambu are oversaturated with respect to Ca-montmorillonite and illite, pointing to a significant interaction with silicate and clay-rich host rocks. The pronounced carbonate undersaturation and elevated p(CO<sub>2</sub>) values in springs from Águas de Contendas and Lambari spa parks suggest the input of deep-seated CO<sub>2</sub> of geogenic origin.

The log activity of  $\text{Ca}^{2+}/(\text{H}^+)^2$  was plotted in a diagram versus the log activity of H<sub>4</sub>SiO<sub>4</sub> using Python 3.13.2 software, based on input parameters including pH, Ca<sup>2+</sup>, and Si concentrations, and assuming a

water temperature of 25 °C (Fig. 3). All spring water samples plot within the kaolinite stability field, suggesting an intermediate to advanced stage of silicate weathering, albeit relatively recent in geological terms.

#### 4.2. Dissolved gas concentrations

Dissolved concentrations of Ar, CO<sub>2</sub>, O<sub>2</sub> and N<sub>2</sub> in spring waters are shown in Table S4 for all sampling points in the two sampling campaigns. Concentrations of dissolved He, Ne, and Ar from copper tube samples are provided in Table 2. In general, dissolved gas concentrations follow this order: CO<sub>2</sub> > N<sub>2</sub> > O<sub>2</sub> > Ar > He > Ne. Concentrations of Ne and Ar are well below the air saturated water (ASW) value in all samples. This can be explained by the fact that noble gases have different solubilities in water, which can lead to fractionation based on their relative solubilities. When magmatic CO<sub>2</sub> bubbles through a water column, the air-derived noble gases preferentially partition into the gas phase. As a result, the remaining water becomes depleted in these components – particularly in lighter noble gases such as <sup>20</sup>Ne and <sup>36</sup>Ar, leading to their observed undersaturation in the residual fluids (Aeschbach-Hertig et al., 2008). The observed positive correlation between O<sub>2</sub> and Ar (Fig. 4) can be explained by the similarity in diffusion coefficients and Henry coefficients, which govern the physics of air/water partitioning for both gases (Weiss, 1970; Mächler et al., 2013). Moreover, the pronounced negative correlations between O<sub>2</sub> and CO<sub>2</sub>, and between Ar and CO<sub>2</sub> suggest mixing between two distinct endmembers, with the CO<sub>2</sub>-enriched component likely originating from a deep source.

All water samples show He concentrations significantly higher than the atmospheric value. This He excess is also apparent in <sup>4</sup>He/<sup>20</sup>Ne values, which are distinctively higher than atmospheric air or ASW in all samples. These observations suggest a considerable presence of deeply-derived, non-atmospheric He (Torgersen and Clarke, 1985; Gilfillan et al., 2008; Gilfillan et al., 2011).

Water from Águas de Contendas (AC-PT) shows a <sup>40</sup>Ar/<sup>36</sup>Ar ratio slightly higher than the respective ASW value. This indicates deep mantle or crustal contribution through the addition of <sup>40</sup>Ar from the radioactive decay of <sup>40</sup>K. The other spring samples exhibit lower <sup>40</sup>Ar/<sup>36</sup>Ar ratios and are near the ASW value.

Seasonal variation in dissolved gas concentrations is evident in the CO<sub>2</sub>/50–N<sub>2</sub>–O<sub>2</sub> ternary plot (Fig. 5), with CO<sub>2</sub> proportions being generally higher in November compared to the same springs in June, while N<sub>2</sub> proportions are correspondingly lower in November. However, no significant seasonal differences are observed in the Águas de

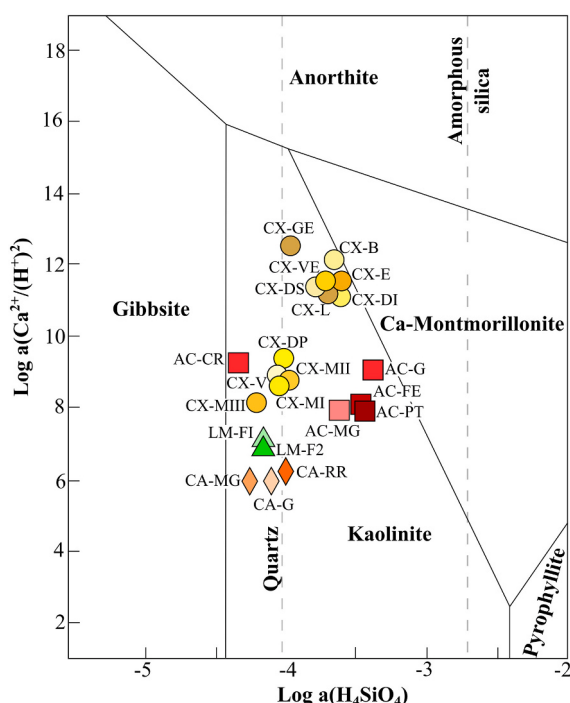


Fig. 3. Diagram of log activity of  $\text{Ca}^{2+}/(\text{H}^+)^2$  versus log activity of H<sub>4</sub>SiO<sub>4</sub> based on input parameters including pH, Ca<sup>2+</sup>, and Si concentrations, at water temperature of 25 °C.

**Table 2**

Helium and argon isotope data with respective uncertainties compared to air saturated water (ASW), as well as  $\delta^{13}\text{C}$  data from literature of  $\text{CO}_2$  for spring water samples and mantle/crustal contribution coefficients for He calculated by Eq. 3.

Sample ID	${}^3\text{He} \times 10^{-16}$ (mol cm $^{-3}$ )	${}^4\text{He} \times 10^{-10}$ (mol cm $^{-3}$ )	${}^{20}\text{Ne} \times 10^{-13}$ (mol cm $^{-3}$ )	${}^{36}\text{Ar} \times 10^{-12}$ (mol cm $^{-3}$ )	${}^{40}\text{Ar} \times 10^{-9}$ (mol cm $^{-3}$ )	${}^3\text{He}/{}^4\text{He} \times 10^{-6}$	${}^3\text{He}/{}^4\text{He}$ (R <sub>c</sub> /R <sub>a</sub> )	${}^4\text{He}/{}^{20}\text{Ne}$	${}^{40}\text{Ar}/{}^{36}\text{Ar}$	Mantle (%)	Crustal (%)	$\delta^{13}\text{C}$ ‰*
AC-PT	14.88 ± 0.51	4.62 ± 0.05	8.87 ± 0.28	11.1 ± 0.21	3.77	3.22 ± 0.10	2.30	520.4 ± 20.8	338.7 ± 1.4	28	72	-0.7
CA-RR	1.63 ± 0.06	2.11 ± 0.02	7.01 ± 0.22	6.02 ± 0.11	1.82	0.77 ± 0.02	0.55	301.0 ± 12.0	301.8 ± 1.2	6	94	-2.8
CX-M2	2.34 ± 0.08	0.49 ± 0.01	6.74 ± 0.22	5.03 ± 0.10	1.54	4.74 ± 0.14	3.39	73.2 ± 2.9	306.8 ± 1.2	42	58	-3.6
LM-F1	0.22 ± 0.01	0.17 ± 0.002	1.21 ± 0.04	1.27 ± 0.02	0.38	1.33 ± 0.04	0.95	137.1 ± 5.5	300.9 ± 1.2	11	89	-3.1
ASW**	0.03	0.02	74.54	46.70	13.91	1.40	1	0.27	298.6			

\*  $\delta^{13}\text{C}(\text{CO}_2)$  values taken from the technical report of [CODEMGE \(2018\)](#).

\*\* Air saturated water at 20 °C.

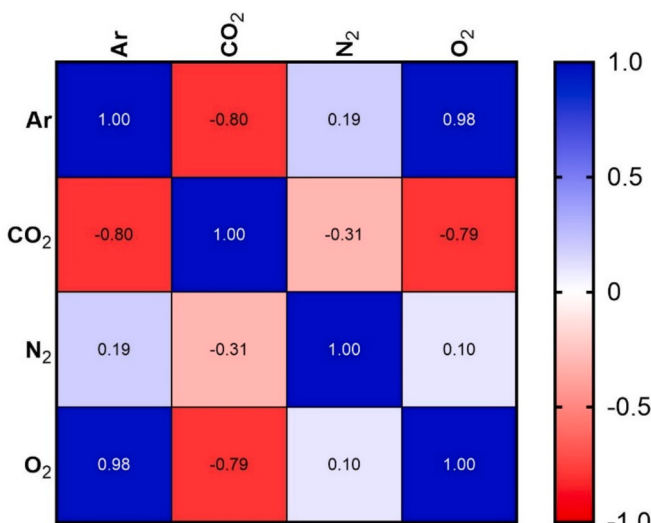


Fig. 4. Correlation matrix for dissolved gas concentrations from June and November 2023 of all sampling areas,  $n = 11$ .

Contendas (AC-PT) sample, suggesting a deeper source with limited interaction with recently recharged water. Furthermore, dissolved gas data were plotted on a  $\text{CO}_2/50-\text{N}_2-\text{He}^*\text{1000}$  ternary plot (Fig. 6) alongside data from previous studies, including thermal waters of Volcano Island (Southern Tyrrhenian Sea) by Capasso and Inguaggiato (1997), soda spring waters of São Tomé and Bioko islands (West Africa) by Aka et al. (2001), carbonic spring deposits of South-Central Australia by Ring et al. (2016) and spring waters of the Southeastern Carpathians (Romania) by Lange et al. (2023). Because atmospheric pressure and water temperature are not available, we assumed an atmospheric pressure of 1 atm and a water temperature of 16 °C for Lange et al. (2023). Thus, the concentration estimates are approximations. The data reveal pronounced variations in the relative proportions of He and  $\text{CO}_2$  among the spring waters of the Water Circuit of Minas Gerais. Samples from Caxambu and Lambari plot close to the signatures of springs from São Tomé (Aka et al., 2001) and Romania (Lange et al., 2023), where both He and  $\text{CO}_2$  are predominantly mantle-derived. In contrast, samples from Águas de Contendas and Cambuquira exhibit significantly higher proportions of He relative to  $\text{CO}_2$  and  $\text{N}_2$ .

#### 4.3. Helium isotopes ( ${}^3\text{He}/{}^4\text{He}$ )

${}^3\text{He}/{}^4\text{He}$  values are reported relative to air (R<sub>a</sub>) according to the

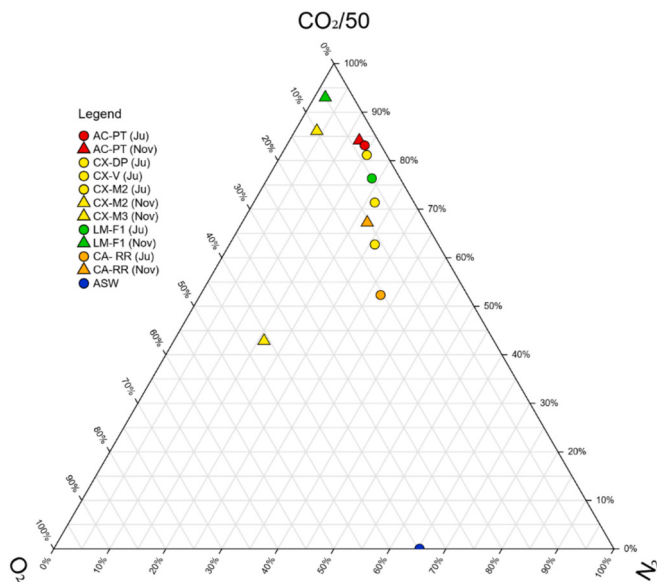


Fig. 5.  $\text{CO}_2/50-\text{N}_2-\text{O}_2$  triangular plot for dissolved concentrations in spring waters from June and November 2023. ASW = Air-saturated water.

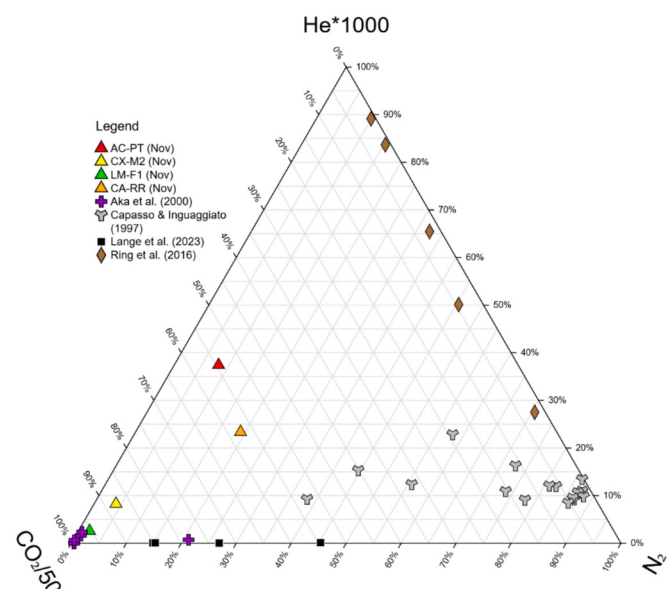


Fig. 6.  $\text{CO}_2/50-\text{N}_2-\text{He}^*\text{1000}$  triangular plot for dissolved concentrations in spring waters from November 2023 compared with data from literature.

method of Craig et al. (1978). Sample  ${}^3\text{He}/{}^4\text{He}$  values were corrected for atmospheric contributions using He/Ne (e.g., Hilton, 1996; Barry et al., 2021) and range from 0.5 to 3.4  $\text{R}_\text{a}$  (Table 1). The two samples from Caxambu (3.4  $\text{R}_\text{a}/\text{R}_\text{a}$ ) and Águas de Contendas (2.3  $\text{R}_\text{a}/\text{R}_\text{a}$ ) show elevated  ${}^3\text{He}/{}^4\text{He}$  – indicating mantle influence, whereas springs from Cambuquira and Lambari show  ${}^3\text{He}/{}^4\text{He}$  values similar to atmospheric ratios. However, all samples exhibit  ${}^4\text{He}$  concentrations significantly higher than those found in air-saturated water (ASW) by at least one order of magnitude. Given that there are no significant sources of He within the atmosphere (Ballentine et al., 2002), and  ${}^4\text{He}$  primarily originates from the radioactive alpha decay of uranium and thorium in the Earth's crust and mantle (Torgersen and Clarke, 1985), this observation suggests that all samples contain very low atmospheric influence, and a significant portion of these waters originate from the deep crust and/or mantle. In Fig. 7 we plot  ${}^3\text{He}/{}^4\text{He} (\text{R}/\text{R}_\text{a})$  versus  ${}^4\text{He}/{}^{20}\text{Ne}$ , together with binary mixing lines between ASW, mantle (8  $\text{R}_\text{a}$ ) and crustal (0.02  $\text{R}_\text{a}$ ) end-members, as well as the highest and lowest regional end-members (Caxambu 3.39  $\text{R}_\text{a}$  and Cambuquira 0.55  $\text{R}_\text{a}$ ). The other two samples plot intermediately between these end-member mixing lines, indicating a mixture of all three (ASW, mantle and crust) end-members. The air-corrected He isotope ratios ( $\text{R}_\text{c}/\text{R}_\text{a}$ ) were used to calculate the fraction of mantle-derived He in the sampled spring water based on the equation by Barry et al. (2021), assuming a binary mixture between mantle and crustal endmembers (Eq. 3):

$$\% \text{Mantle He} = \left( \text{R}_\text{c}/\text{R}_\text{a} - {}^3\text{He}/{}^4\text{He}_{\text{Crust}} \right) / \left( {}^3\text{He}/{}^4\text{He}_{\text{Mantle}} - {}^3\text{He}/{}^4\text{He}_{\text{Crust}} \right) \quad (3)$$

where,  ${}^3\text{He}/{}^4\text{He}_{\text{Mantle}} = 8 \text{ R}_\text{a}$ ,  ${}^3\text{He}/{}^4\text{He}_{\text{Crust}} = 0.05 \text{ R}_\text{a}$  (Graham, 2002; Morrison and Pine, 1955).

Results of this calculation point to a significant He mantle contribution of 42 % for the Caxambu sample and 28 % for the sample from Águas de Contendas, while samples from Cambuquira and Lambari show more negligible He mantle contributions under 15 %.

Mayrink II spring samples from Caxambu display the highest  ${}^3\text{He}/{}^4\text{He}$  of all samples. Caxambu is situated adjacent to the Caxambu dextral transcurrent shear zone (CXSZ in Fig. 1). The CXSZ is a dextral strike slip-shear zone with approximately 150 km of extension in the NE-SW direction, with a maximum horizontal displacement of approximately 20 km and an estimated age of 570 to 550 Ma (Trouw et al., 2008). The shear zone intersects all preexisting structures within the country rocks and hosts mylonite, believed to have formed under conditions corresponding to the upper greenschist to lower amphibolite facies (Trouw et al., 2013). When plotting  ${}^3\text{He}/{}^4\text{He}$  against distance to this fault zone, it is clear that the  ${}^3\text{He}/{}^4\text{He}$  consistently decreases with

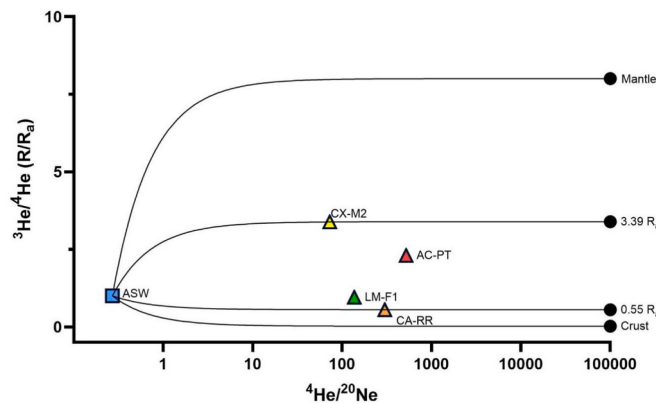


Fig. 7.  $\text{R}/\text{R}_\text{a}$  vs.  ${}^4\text{He}/{}^{20}\text{Ne}$  diagram for samples and air saturated water (ASW). Solid lines represent binary mixing between ASW and mantle end-member (8  $\text{R}_\text{a}$ ), the highest sampled end-member (Caxambu, 3.39  $\text{R}_\text{a}$ ), and the lowest sampled end-member (Cambuquira, 0.55  $\text{R}_\text{a}$ ) and a crustal end-member (0.02  $\text{R}_\text{a}$ ).

increasing distance from the fault (Fig. 8). Hence, it is postulated that this fault zone may serve as a major conduit for the ascent of mantle-derived He and fluids to the surface, with the mantle He undergoing gradual dilution by crustal components as it migrates through the basement over increasing distances, a pattern previously observed at other locations by Kennedy and Van Soest (2007), Barry et al. (2020), Umeda and Ninomiya (2009), Klemperer et al. (2013), Zhang et al. (2021) and Klemperer et al. (2022).

#### 4.4. Relationship of helium isotopes to $\text{CO}_2$ concentrations and $\delta^{13}\text{C} (\text{CO}_2)$

$\text{CO}_2$  concentrations show a narrow range and no correlation with  $\text{CO}_2/{}^3\text{He}$ , indicating that  $\text{CO}_2$  addition or loss has little influence on  $\text{CO}_2/{}^3\text{He}$  values (Barry et al., 2019, 2022). Furthermore, Fig. 9 shows the relation between  $\text{CO}_2/{}^3\text{He}$  and  $\delta^{13}\text{C} (\text{CO}_2)$  in spring samples. In addition, we also plot end-member data for mid-ocean ridge basalts (MORBs), organic sediments (Sediments) and marine limestone carbonates (Carbonates) as reported by Sano and Marty (1995) and Barry et al. (2021). Data of  $\delta^{13}\text{C} (\text{CO}_2)$  were taken from the technical report of CODEMGE (2018), based on  $\text{CO}_2$  extracted from water samples collected in 2018 and analyzed using accelerator mass spectrometry. Combined  $\text{CO}_2/{}^3\text{He}$  and  $\delta^{13}\text{C} (\text{CO}_2)$  data plot close to the mantle-carbonate binary mixing line, indicating an admixture of mantle and carbonate He and C. We note however that there are no confirmed reports of carbonate rocks in the area, so it is possible that this isotopically high C signature could be related to Paleoproterozoic carbonates. For instance, the Gandarela Formation within the Minas Supergroup is predominantly composed of shallow-water carbonates, dated to  $2.42 \pm 0.02 \text{ Ga}$  (Babinski et al., 1995; Sial et al., 2000). The  $\delta^{13}\text{C}$  signatures of these rocks vary from  $-1.6$  to  $+0.4 \text{ ‰}_{\text{PPDB}}$ , which are close to the  $\delta^{13}\text{C} (\text{CO}_2)$  signatures measured in the analyzed spring waters (Sial et al., 2000). This interpretation is consistent with observed helium signatures, whereby  ${}^3\text{He}/{}^4\text{He}$  is modified by  ${}^4\text{He}$  addition during migrating through the crust to the surface. However, our results suggest that the origins of  $\text{CO}_2$  and He in the sampled spring waters differ significantly and thus  $\text{CO}_2$  and He appear to be decoupled.

Data of Ferraz et al. (2019) from gas samples of offshore petroleum accumulations from the Santos Basin (approximately 400 km of distance from the Water Circuit) are also plotted on Fig. 9. In contrast to our data, these signatures show a strong influence of mantle fluids, probably

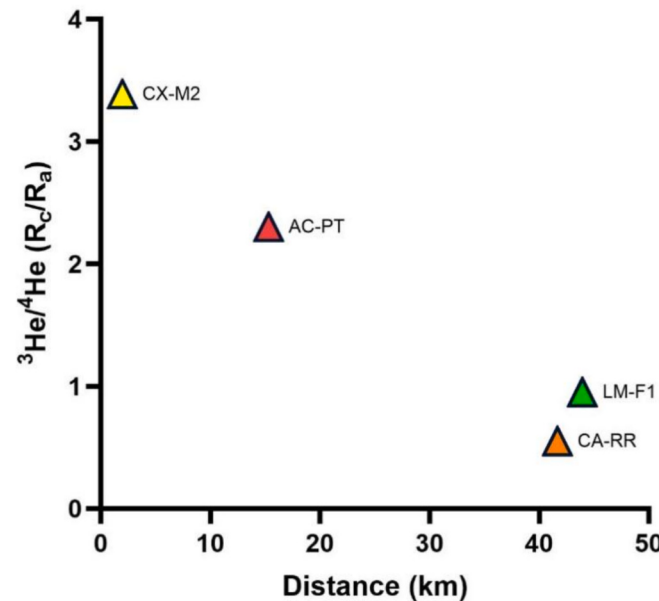
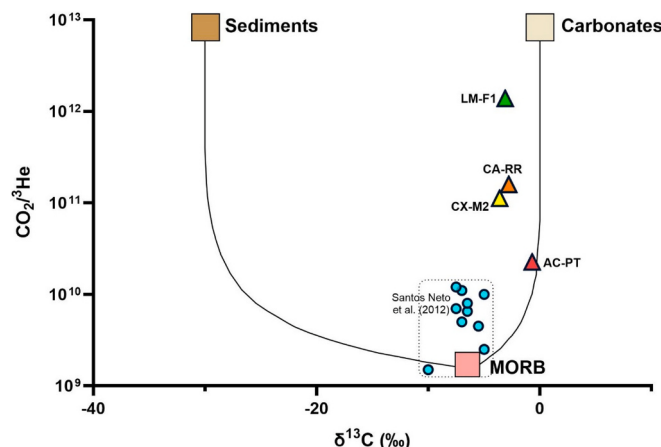


Fig. 8. Ratios of  ${}^3\text{He}/{}^4\text{He} (\text{R}_\text{c}/\text{R}_\text{a})$  plotted against distance from CXSZ fault.



**Fig. 9.**  $\text{CO}_2/\text{He}^3$  ratios vs  $\delta^{13}\text{C}(\text{CO}_2)$  values for gas samples together with mantle (MORB), carbonate (Carbonates) and sediment organic (Sediments)  $\text{CO}_2$  end-members from Sano and Marty (1995) and Barry et al. (2022).

related to thinning of the continental crust on the São Paulo Plateau, enabling mantle-derived materials to rise to the upper crustal levels (Ferraz et al., 2019). This shows that  $\text{CO}_2$  from the Water Circuit primarily originated from sources beyond  $\text{CO}_2$  from the Santos Basin.

## 5. Implications on $\text{CO}_2$ and helium origins and regional geology

Anorogenic magmatism is characterized by the generation of small volumes of alkaline magmas and related to changes in plate dynamics. Provinces of anorogenic magmatism are situated above deep, pre-existing structures, that have been geological active over time (Ferroni et al., 2018; Bailey and Woolley, 2005). In Brazil, the most significant Phanerozoic alkaline provinces are located near the northern border of the Paraná Basin and along the continental margin (Almeida et al., 1981; Ulbrich and Gomes, 1981). An important aspect of these alkaline provinces is their relationship with crustal structures, as the intrusions are controlled, aligned and elongated according to pre-existing weakness zones of crystalline basement (de Almeida, 1983; Riccomini et al., 2005; Ferroni et al., 2018). As previously mentioned, mafic dikes and Cenozoic alkaline intrusions from the Cretaceous and Paleogene are also present in the stratigraphic framework of the Water Circuit region. Here, the Caxambu intrusion is particularly significant, forming the Morro de Caxambu, consisting of breccias, trachytes, and aphanitic syenites (CODEMGE, 2018). The earlier mentioned Caxambu transcurrent shear

zone (CXSZ), cutting through the region-oriented NE-SW, is a dextral strike-slip shear zone extending approximately 150 km, with a maximum horizontal displacement of approximately 20 km in its central portion (Fig. 1). The shear zone intersects all other structures in the surrounding rocks including the Morro do Caxambu intrusions (Trouw et al., 2003 and 2008; Trouw et al., 2013).

Recent findings from the northern continental shelf of the South China Sea indicates the presence of abundant mantle helium and  $\text{CO}_2$  with areas of crustal thinning, with thickness less than 26 km and elevated thermal flow above  $61.2 \text{ mW/m}^2$ . This region is marked by complex fault systems (Li et al., 2008), which are observed in the offshore portion of the schematic geological profile of Southeastern Brazil (Fig. 10). Ferraz et al. (2019) and Gamboa et al. (2019) documented the injection of mantle-derived  $\text{CO}_2$ -rich material in the offshore Santos Basin, specifically in the São Paulo Plateau, approximately 400 km from the Water Circuit. The thinning of the crust and the zones of weakness in the lithosphere (i.e., faults and fractures), facilitated the ascent of this material to higher levels, where it became trapped in reservoirs.

In the continental portion of the Water Circuit of Minas Gerais, there is no crustal thinning to explain the same event. We estimate the crustal thickness in the study area to be between 37.5 and 40.4 km, based on interpolation of data from Assumpção et al. (2002) and Assumpção et al. (2013). The observed differences in  $\text{CO}_2/\text{He}^3$  ratios vs  $\delta^{13}\text{C}(\text{CO}_2)$  between Santos and Campos Basins (Ferraz et al., 2019) and our study area (Fig. 9) clearly show a significant depletion of mantle-derived He in the latter. For this reason, we interpret major fault segments of the CXSZ as conduits, which enabled  $\text{CO}_2$ -rich magmatic material to ascend and enrich the springs of the Water Circuit region (Ferroni et al., 2018).

Comparisons of strontium isotopic signatures ( $^{87}\text{Sr}/^{86}\text{Sr}$ ) obtained from the mineral water samples with those of regional rocks (quartzite, schist, amphibolite and alkaline volcanic rock) were presented in CODEMGE (2018). Notably, a strong correspondence was identified between the isotopic Sr signature of the waters from Caxambu Park ( $^{87}\text{Sr}/^{86}\text{Sr}$  = between 0.7061 and 0.7069) and the alkaline rocks of the Morro do Caxambu alkaline volcanic structure ( $^{87}\text{Sr}/^{86}\text{Sr}$  = between 0.7076 and 0.7255). The isotopic signatures of the mineral waters from Cambuquira, Contendas, and Lambari were found to correspond to those of regional rocks (quartzite, schist, and amphibolite) associated with their respective aquifers.

Crustal fracture zones, especially major shear zones such as the Caxambu Shear Zone, likely control the distribution of major vertical conduits for  $\text{CO}_2$  and He migration. Previous studies have shown that the  $\delta^{18}\text{O}$  and  $\delta^2\text{H}$  isotopic signatures of the waters are characteristic of

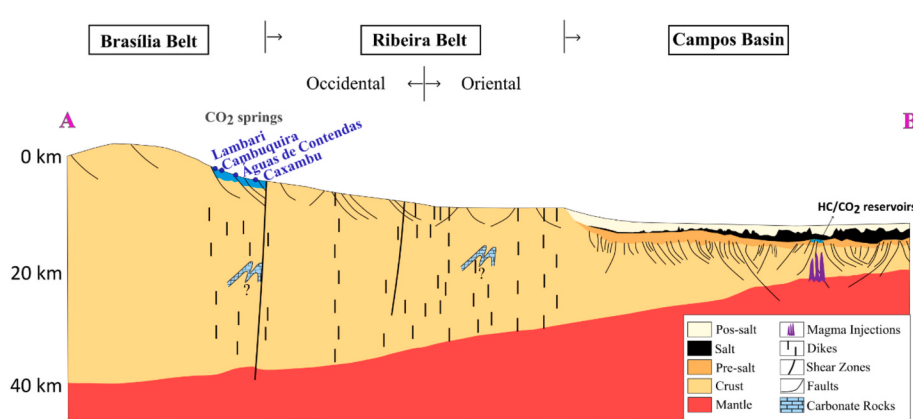


**Fig. 10.** Illustrative geological cross-section. The offshore section was adapted from Ros et al. (2017) and Gamboa et al. (2019), while the onshore section was modified from Zalán et al. (2011), Assumpção et al. (2013) and Ferroni et al. (2018). Note that the thinning of the crust in the offshore section enabled the formation of hydrocarbon- $\text{CO}_2$  (HC/ $\text{CO}_2$ ) reservoirs, while in the onshore section, the enrichment of  $\text{CO}_2$  was facilitated by the combination of the shear zone, faults and dikes. We assume the presence of crustal carbonate rocks in contact with the shear zones as  $\text{CO}_2/\text{He}^3$  and  $\delta^{13}\text{C}(\text{CO}_2)$  signatures in spring waters point to a significant contribution of carbonate-derived  $\text{CO}_2$ .

ancient meteoric waters that have undergone deep circulation (CODEMGE, 2018). This suggests that the transported CO<sub>2</sub> from its deep source to the surface involves migration as a separate gas phase, with dissolution into meteoric waters at considerable depths.

Recent studies (Gernon et al., 2023, 2024) have also demonstrated that alkaline magmas and kimberlites along rifted continental margins most likely originate from convective instabilities that develop after continental breakup. These studies suggest that the steep lithosphere–asthenosphere boundaries formed during rifting can migrate hundreds of kilometers inland from rift zones. Such instabilities can persist for tens of millions of years, leading to the delamination of the cratonic lithosphere's thermal boundary layer. As a result, the displaced basal lithosphere is replaced by a hot, upwelling mixture of asthenosphere and recycled volatile-rich lithospheric mantle, triggering decompression partial melting. When this melt interacts with carbonate-rich lithologies in the lower crust, decarbonation reactions may release significant amounts of CO<sub>2</sub>.

However, considering measured <sup>3</sup>He/<sup>4</sup>He and CO<sub>2</sub>/<sup>3</sup>He in our samples and the inferred mantle contributions from that data, it is assumed that fractions of He and CO<sub>2</sub> are constantly being supplied from the mantle. If mantle-derived He would be stored over a long period, significantly lower <sup>3</sup>He/<sup>4</sup>He ratios would be expected due to the accumulation of radiogenic <sup>4</sup>He from the crust (Pinti and Marty, 1998; Barry et al., 2025). From this perspective, fractions of the CO<sub>2</sub> in the Water Circuit region share the same origin as the CO<sub>2</sub> found in the Santos Basin, both being a consequence of the breakup of Gondwana.

## 6. CO<sub>2</sub> flux through springs

The minimum CO<sub>2</sub> flux from the study region into the surface system was estimated by multiplying the dissolved CO<sub>2</sub> concentration measured in each spa town park by the total discharge (L/s) of all springs in the respective parks, as reported in CODEMGE (2018). The data from CODEMGE (2018) provides discharge values for each spring in the four parks over several years, from which the average discharge for each spring was calculated. For springs where CO<sub>2</sub> concentration was not measured, the average CO<sub>2</sub> concentration measured in nearby springs, within the same park, was assumed to be representative. Thus, the CO<sub>2</sub> flux into the surface system from all springs in the four parks was estimated to be  $4.26 \times 10^6$  mol year<sup>-1</sup>, with contributions of  $1.61 \times 10^6$  mol year<sup>-1</sup> from Caxambu,  $4.6 \times 10^5$  mol year<sup>-1</sup> from Cambuquira,  $7.51 \times 10^5$  mol year<sup>-1</sup> from Águas de Contendas and  $1.44 \times 10^6$  mol year<sup>-1</sup> from Lambari. These findings represent a minor yet consistent contribution to the CO<sub>2</sub> budget when compared to the reported CO<sub>2</sub> flux estimations of  $3 \times 10^8$  mol year<sup>-1</sup> from geothermal springs of the Colorado Rocky Mountains in the western USA (Karlstrom et al., 2013), CO<sub>2</sub> flux estimations of  $\sim 10^9$  mol year<sup>-1</sup> from northern New Mexico (Goff and Janik, 2002), CO<sub>2</sub> flux estimations of  $\sim 10^{11}$  mol year<sup>-1</sup> from the Yellowstone region of Wyoming (Werner and Brantley, 2003), CO<sub>2</sub> flux estimations of  $2.1 \times 10^{11}$  mol year<sup>-1</sup> from the Tuscan Roman Degassing Structure and the Campanian Degassing Structure in Italy (Frondini et al., 2019), and CO<sub>2</sub> flux from mid-ocean ridges and continental volcanoes estimated to be  $\sim 10^{12}$  mol year<sup>-1</sup> (Kerrick, 2001). Thus, our data provides an essential baseline for future carbon sequestration studies in Brazil, given the absence of prior data of this nature for the region.

## 7. Conclusions

This study represents the first attempt to use noble gas abundance and isotope data to reveal origins and transport mechanisms of CO<sub>2</sub> and He from the springs of the Water Circuit of Minas Gerais. Due to the significantly higher He concentrations, <sup>3</sup>He/<sup>4</sup>He, and <sup>4</sup>He/<sup>20</sup>Ne values in the water samples compared to the respective atmospheric values, a deep origin and the gradual accumulation of radiogenic <sup>4</sup>He in the waters is assumed. Air-corrected <sup>3</sup>He/<sup>4</sup>He values of the samples indicate an admixture of crustal and mantle volatile contribution. The spring

water of the Caxambu park, situated adjacent to the Caxambu dextral transcurrent shear zone, showed the highest <sup>3</sup>He/<sup>4</sup>He values and the highest mantle contribution of all analyzed springs (42%). A consistent <sup>3</sup>He/<sup>4</sup>He decrease with increasing distance to the Caxambu shear zone was observed, suggesting that Caxambu shear zone and associated faults serve as a conduit for the ascent of mantle-derived He and CO<sub>2</sub>. We surmise that major fault segments along the Caxambu shear zone serve as preferential pathways for upflow of mantle-derived CO<sub>2</sub> and He from depth continuously enriching the springs of the Water Circuit region. However, our results indicate a significant decoupling between the sources of He and CO<sub>2</sub>, implying a lower mantle-derived contribution to the CO<sub>2</sub> flux. CO<sub>2</sub>/<sup>3</sup>He and δ<sup>13</sup>C (CO<sub>2</sub>) signatures point to significant crustal-carbonate contribution for the CO<sub>2</sub> although no carbonate lithologies have been confirmed in the region to date.

## CRediT authorship contribution statement

**Hendryk Gemeiner:** Writing – review & editing, Writing – original draft, Visualization, Validation, Software, Methodology, Investigation, Formal analysis, Data curation, Conceptualization. **Hung Kiang Chang:** Writing – review & editing, Writing – original draft, Visualization, Validation, Supervision, Resources, Project administration, Methodology, Investigation, Funding acquisition, Conceptualization. **Larissa Neris Alcara:** Writing – review & editing, Visualization, Investigation, Formal analysis, Data curation. **Marcelo Martins Reis:** Writing – original draft, Project administration, Investigation, Formal analysis, Data curation, Conceptualization. **Peter H. Barry:** Writing – review & editing, Visualization, Validation, Investigation, Funding acquisition. **Amauri Antonio Menegário:** Writing – review & editing, Project administration, Methodology, Formal analysis.

## Declaration of Competing Interest

The authors declare that they have no known competing financial interests or personal relationships that could have appeared to influence the work reported in this paper.

## Acknowledgements

Funding was provided by FUNDUNESP (3446/2023) and CNPq. PHB acknowledges NSF awards 2121637, 2151120, 2152551, 2232531, 2321494, and 2319897. The authors deeply thank the Agency for Development of the State of Minas Gerais (Companhia de Desenvolvimento de Minas Gerais – CODEMGE), especially Mr. Pedro Paulo Moraes Cunha and Mr. Filipe Lopes Chaves, for giving access to the field sites and all given support during sampling. Furthermore, the authors highly thank Mr. José Carlos Laendl and Mr. Marcos Perdiza from LEBAC – UNESP Rio Claro for field and technical support. We thank Don Porcelli for editorial handling and Francesco Frondini, Galip Yuce as well as an anonymous reviewer for providing constructive and insightful feedback throughout the review process.

## Appendix A. Supplementary data

Supplementary data to this article can be found online at <https://doi.org/10.1016/j.chemgeo.2025.122939>.

## Data availability

Data will be made available on request.

## References

Aeschbach-Hertig, W., Solomon, D.K., 2013. Noble Gas Thermometry in Groundwater Hydrology, 81–122. [https://doi.org/10.1007/978-3-642-28836-4\\_5](https://doi.org/10.1007/978-3-642-28836-4_5).

- Aeschbach-Hertig, W., El-Gamal, H., Wieser, M., Palcsu, L., 2008. Modeling excess air and degassing in groundwater by equilibrium partitioning with a gas phase. *Water Resour. Res.* 44 (8).
- Aka, F.T., Kusakabe, M., Nagao, K., Tanyileke, G., 2001. Noble gas isotopic compositions and water/gas chemistry of soda springs from the islands of Bioko, São Tomé and Annobon, along with Cameroon Volcanic Line, West Africa. *Appl. Geochem.* 16, 323–338. [https://doi.org/10.1016/S0883-2927\(00\)00037-8](https://doi.org/10.1016/S0883-2927(00)00037-8).
- Alita, T.T., 2017. Alteração hidrotermal tipo Skarn do contato intrusivo do Gabro de Apiaí e Metasedimentos da Formação Gorutuba: Município de Apiaí-SP. Dissertation. Campinas State University, p. 59.
- de Almeida, F.F., 1983. Relações tectónicas das rochas alcalinas mesozóicas da região meridional da Plataforma Sul-Americana. *Revista Brasileira de Geociências* 13 (3), 139–158. Available at: <https://scholar.archive.org/work/gtugm2zhyngobbehwlefkaj22i/access/wayback/http://www.ppegeo.igc.usp.br:80/index.php/rbg/article/download/12148/11694>.
- Almeida, F.F.M., Hasui, Y., de Brito Neves, B.B., Fuck, R.A., 1981. Brazilian structural provinces: an introduction. *Earth Sci. Rev.* 17, 1–29. [https://doi.org/10.1016/0012-8252\(81\)90003-9](https://doi.org/10.1016/0012-8252(81)90003-9).
- Almeida, J.C.H., Heilbron, M.C.P.L., da Silva, R., Júnior, D.D.L.M., Tetzner, W., 2013. Guia de campo na Área Continental do Alto de Cabo Frio. *Bol. Geociências Petrobras* 21, 325–355.
- Almeida, F.F.M., Amaral, G., Cordani, U., Kawashita, K., 1973. The Precambrian Evolution of South America Cratonic Margin South of Amazon River, in: The South Atlantics, Spring Boston, 411–446. [https://doi.org/10.1007/978-1-4684-3030-1\\_11](https://doi.org/10.1007/978-1-4684-3030-1_11).
- Assumpção, M., James, D., Snoke, A., 2002. Crustal thicknesses in SE Brazilian Shield by receiver function analysis: Implications for isostatic compensation. *J. Geophys. Res. Solid Earth* 107 (B1), ESE-2. <https://doi.org/10.1029/2001JB000422>.
- Assumpção, M., Feng, M., Tassara, A., Julia, J., 2013. Models of crustal thickness for South America from seismic refraction, receiver functions and surface wave tomography. *Tectonophysics* 609, 82–96. <https://doi.org/10.1016/j.tecto.2012.11.014>.
- Babinski, M., Chemale Jr., F., Van Schmus, W.R., 1995. The PB/PB age of the minas supergroup carbonate rocks, quadrilatero Ferrifero, Brazil. *Precambrian Res.* 72 (3–4), 235–245. [https://doi.org/10.1016/0030-9268\(94\)00091-5](https://doi.org/10.1016/0030-9268(94)00091-5).
- Bailey, D.K., Woolley, A.R., 2005. Repeated, synchronous magmatism within Africa: timing, magnetic reversals, and global tectonics. *Spc. Pap. Geol. Soc. Am.* 388, 365.
- Ballentine, C.J., Burnard, P.G., 2002. Production, release and transport of noble gases in the continental crust. In: Porcelli, D., Ballentine, C.J., Wieler, R. (Eds.), *Noble Gases in Geochemistry*. Mineralogical Society of America, Washington D.C., pp. 481–538. <https://doi.org/10.2138/rmg.2002.47.12>.
- Ballentine, C.J., Burgess, R., Marty, B., 2002. Tracing fluid origin, transport and interaction in the crust. In: Porcelli, D., Ballentine, C.J., Wieler, R. (Eds.), *Noble Gases in Geochemistry*. Mineralogical Society of America, Washington, vol. D.C., pp. 271–409. <https://doi.org/10.2138/rmg.2002.47.13>.
- Barry, P.H., Hilton, D.R., Fischer, T.P., De Moor, J.M., Mangasini, F., Ramirez, C., 2013. Helium and carbon isotope systematics of cold “mazuku” CO<sub>2</sub> vents and hydrothermal gases and fluids from Rungwe Volcanic Province, southern Tanzania. *Chem. Geol.* 339, 141–156. <https://doi.org/10.1016/j.chemgeo.2012.07.003>.
- Barry, P.H., De Moor, J.M., Giovannelli, D., Schrenk, M., Hummer, D.R., Lopez, T., Pratt, C.A., Segura, Y.A., Battaglia, A., Beaudry, P., Bini, G., 2019. Forearc carbon sink reduces long-term volatile recycling into the mantle. *Nature* 568 (7753), 487–492. <https://doi.org/10.1038/s41586-019-1131-5>.
- Barry, P.H., Negrete-Aranda, R., Spelz, R.M., Seltzer, A.M., Bekaert, D.V., Virrueta, C., Kulongsoski, J.T., 2020. Volatile sources, sinks and pathways: a helium-carbon isotope study of Baja California fluids and gases. *Chem. Geol.* 550, 119722. <https://doi.org/10.1016/j.chemgeo.2020.119722>.
- Barry, P.H., Bekaert, D.V., Krantz, J.A., Halldórsson, S.A., de Moor, J.M., Fischer, T.P., Werner, C., Kelly, P.J., Seltzer, A.M., Franz, B.P., Kulongsoski, J.T., 2021. Helium-carbon systematics of groundwaters in the Lassen Peak Region. *Chem. Geol.* 584, 120535. <https://doi.org/10.1016/j.chemgeo.2021.120535>.
- Barry, P.H., De Moor, J.M., Chiodi, A., Aguilera, F., Hudak, M.R., Bekaert, D.V., Turner, S.J., Curtice, J., Seltzer, A.M., Jessen, G.L., Osses, E., Blamey, J.M., Amenabar, M.J., Selci, M., Cascone, M., Bastianoni, A., Nakagawa, M., Filippovich, R., Bustos, E., Schrenk, M.O., Buongiorno, J., Ramírez, C.J., Rogers, T.J., Lloyd, K.G., Giovannelli, D., 2022. The helium and carbon isotope characteristics of the Andean Convergent Margin. In: *Frontiers in Earth Science*, 10, Special Issue: Volcanism in the Central Volcanic Zone of the Andes. <https://doi.org/10.3389/feart.2022.897267>.
- Barry, P.H., De Moor, J.M., Broadley, M.W., Seltzer, A.M., Bekaert, D.V., Patil, K., Bartels, C.G.E., Young, E.D., Longworth, B.E., Barosa, B., Bastianoni, A., 2025. Carbon, nitrogen, and noble gas isotopes reveal deep volatile signatures in thermal springs in the Central Volcanic Zone (CVZ) of the Andes. *Earth Planet. Sci. Lett.* 651, 119169. <https://doi.org/10.1016/j.epsl.2024.119169>.
- Beato, D.A.C., Oliveira, F.A.R., Viana, H.S., 1998. Projeto Circuito das Águas do Estado de Minas Gerais: estudos geoambientais das fontes hidrominerais de Cambuquira, Caxambu, Conceição do Rio Verde, Lambari e São Lourenço, Belo Horizonte, SEME/CPHM, p. 142.
- Bekaert, D.V., Barry, P.H., Broadley, M.W., Byrne, D.J., Marty, B., Ramírez, C.J., de Moor, J.M., Rodriguez, A., Hudak, M.R., Sunhas, A.V., Halldórsson, S.A., Jessen, G. L., Blamey, J.M., Stefánsson, A., Cracausi, A., Lloyd, K.G., Giovannelli, D., Seltzer, A. M., 2023. Ultrahigh-precision noble gas isotope analyses reveal pervasive subsurface fractionation in hydrothermal systems. *Sci. Adv.* 9, 2566. <https://doi.org/10.1126/sciadv.adg2566>.
- Campos Neto, M.C., Cabo, R., 2000. Terrane accretion and upward extrusion of high-pressure granulites in the Neoproterozoic nappes of Southeast Brazil. *Petrological and structural constraints. Tectonics* 19, 669–687. <https://doi.org/10.1029/1999TC000065>.
- Campos Neto, M.C., Figueiredo, M.C.H., 1995. The Rio Doce Orogeny, Southeastern Brazil. *J. S. Am. Earth Sci.* 8, 143–162. [https://doi.org/10.1016/0895-9811\(95\)0002-W](https://doi.org/10.1016/0895-9811(95)0002-W).
- Cartwright, I., Weaver, T., Tweed, S., Ahearne, D., Cooper, M., Cooper, M., Czapnik, K., Tranter, J., 2002. Stable isotope geochemistry of cold CO<sub>2</sub>-bearing mineral spring waters, Daylesford, Victoria, Australia: sources of gas and water and links with waning volcanism. *Chem. Geol.* 185, 71–91. [https://doi.org/10.1016/S0009-2541\(01\)00397-7](https://doi.org/10.1016/S0009-2541(01)00397-7).
- CODEMGE, 2018. SIGA, Circuito das Águas: Caracterização geoambienteal, geológica, hidrogeológica e hidrogeoquímica do Circuito das Águas de Minas Gerais, com ênfase nos parques hidrominerais de Caxambu, Cambuquira, Marimbeiro, Contendas e Lambari, first ed. Companhia de Desenvolvimento de Minas Gerais, Belo Horizonte. Available at: <http://www.codemge.com.br/wp-content/uploads/2019/07/siga-circuito-das-aguas-100719.pdf>.
- Cordani, U.G., 1973. Evolução geológica pré-cambriana da faixa costeira do Brasil entre Salvador e Vitória. Habilitation Thesis. University of São Paulo, Brazil, p. 80. <https://doi.org/10.11606/T.44.2013.tde-07112013-151714>.
- Cordani, U.G., Ramos, V.A., Fraga, L.M., Cegarra, M., Delgado, I., Souza, K.G.D., Gomes, F.E.M., Schobbenhaus, C., 2016. Tectonic map of South America= Mapa tectónico da América do Sul. CGMW-CPRM-SEGEMAR. ISBN 978-2-917310-26-7. doi: 10.14682/2016TEMSA.
- Corrales, F.P., 2019. Evolução geotectônica dos stocks Neoproterozoicos Marceleza e Leopoldina, remanescentes de arcos magnéticos continentais nos Orógenos Ribeira e Araçuaí: implicações geotectônicas na Província Mantiqueira. Doctoral Thesis., Rio de Janeiro State University, p. 219. <http://www.btdt.uerj.br/handle/1/17180>.
- Costa, N.B.D.O.R., 1996. Projeto Circuito das águas. Estudos Geotécnicos de Caxambu, CPRM, Minas Gerais.
- Craig, H., Lupton, J.E., Horibe, Y., 1978. A mantle helium component in circum-Pacific volcanic gases: Hakone, the Marianas, and Mt. Lassen. In: Alexander, E.V., Ozima, M. (Eds.), *Advances in Earth and Planetary Sciences*, 3. Terrestrial Rare Gases. Center for Academic Publications, Japan Scientific Press, Tokyo, pp. 3–16. <https://doi.org/10.1007/978-94-010-9828-1-1>.
- Damatto, S.R., 2021. Inorganic Chemical Composition by X-Ray Fluorescence Spectrometry of the Mineral Waters from the Minas Gerais Water Circuit, Brazil. *Braz. J. Radiat. Sci.* 9, 1–19. <https://doi.org/10.15392/bjrjs.v9i7A.1528>.
- Ebert, H., 1971. Os Paraibides entre São João do Rei, Minas Gerais e Itapira, São Paulo, e a bifurcação entre Paraibides e Araxaldes. In: *Congr. Bras. Geologia*, 25, São Paulo, 1971, 1. Boletim Especial São Paulo, SBG, pp. 177–178.
- Ferraz, A., Gamboa, L., Neto, E.V.D.S., Baptista, R., 2019. Crustal structure and CO<sub>2</sub> occurrences in the Brazilian basins. In: Interpretation. Speacial Section Wastewater and CO<sub>2</sub> Injection, 7, pp. 37–45. <https://doi.org/10.1190/INT-2019-0038.1>.
- Ferroni, F.R., Mello, C.L., Destro, N., 2018. Tectonic control on the Cabo Frio anorogenic magmatic lineament, Southeastern Brazil. *J. S. Am. Earth Sci.* 83, 37–54. <https://doi.org/10.1016/j.james.2017.11.001>.
- Frondini, F., Cardellini, C., Caliro, S., Beddini, G., Rosiello, A., Chioldini, G., 2019. Measuring and interpreting CO<sub>2</sub> fluxes at regional scale: the case of the Apennines, Italy. *J. Geol. Soc.* 176 (2), 408–416. <https://doi.org/10.1144/jgs2017-16>.
- Gamboa, L., Ferraz, A., Baptista, R., Santos Neto, E.V., 2019. Geotectonic Controls on CO<sub>2</sub> Formation and distribution Processes in the Brazilian Pre-Salt Basins. *Geosciences* 9, 252. <https://doi.org/10.3390/geosciences9060252>.
- Gemeiner, H., Teramoto, E.H., Veroslavsky, G., Chang, H.K., 2025. Using Dissolved Noble gases to Characterize the Groundwaters of the Southern Portion of the Guarani Aquifer System at the Brazil-Uruguay Border Region. *Sci. Total Environ.* 966, 178690. <https://doi.org/10.1016/j.scitotenv.2025.178690>.
- Geron, T.M., Jones, S.M., Brune, S., Hincks, T.K., Palmer, M.R., Schumacher, J.C., Glerum, A., 2023. Rift-induced disruption of cratonic keels drives kimberlite volcanism. *Nature* 620 (7973), 344–350. <https://doi.org/10.1038/s41586-024-07717-1>.
- Geron, T.M., Hincks, T.K., Brune, S., Braun, J., Jones, S.M., Keir, D., Glerum, A., 2024. Coevolution of craton margins and interiors during continental break-up. *Nature* 632 (8024), 327–335. <https://doi.org/10.1038/s41586-024-07717-1>.
- Gilfillan, S.M., Ballantine, C.J., Holland, G., Blagburn, D., Lollar, B.S., Stevens, S., Schoell, M., Cassidy, M., 2008. The noble gas geochemistry of natural CO<sub>2</sub> gas reservoirs from the Colorado Plateau and Rocky Mountain provinces, USA. *Geochim. Cosmochim. Acta* 72, 1174–1198. <https://doi.org/10.1016/j.gca.2007.10.009>.
- Gilfillan, S.M., Wilkinson, M., Haszeldine, R.S., Shipton, Z.K., Nelson, S.T., Poreda, R.J., 2011. He and Ne as tracers of natural CO<sub>2</sub> migration up a fault from a deep reservoir. *Int. J. Greenhouse Gas Control* 5, 1507–1516. <https://doi.org/10.1016/j.ijggc.2011.08.008>.
- Gilfillan, S.M.V., Györe, D., Flude, S., Johnson, G., Bond, C.E., Hicks, N., Lister, R., Jones, D.G., Kremer, Y., Haszeldine, R.S., Stuart, F.M., 2019. Noble gases confirm plume-related mantle degassing beneath Southern Africa. *Nat. Commun.* 10, 5028. <https://doi.org/10.1038/s41467-019-12944-6>.
- Goff, F., Janik, C.J., 2002. Gas geochemistry of the Valles caldera region, New Mexico and comparisons with gases at Yellowstone, Long Valley and other geothermal systems. *J. Volcanol. Geotherm. Res.* 116 (3–4), 299–323. [https://doi.org/10.1016/S0377-0273\(02\)00222-6](https://doi.org/10.1016/S0377-0273(02)00222-6).
- Graham, D.W., 2002. Noble gas isotope geochemistry of mid-ocean ridge and ocean island basalts: Characterization of mantle source reservoirs. *Rev. Mineral. Geochem.* 47, 247–317. <https://doi.org/10.2138/rmg.2002.47.8>.
- Györe, D., Pujol, M., Gilfillan, S.M., Stuart, F.M., 2021. Noble gases constrain the origin, age and fate of CO<sub>2</sub> in the Vaca Muerta Shale in the Neuquén Basin (Argentina). *Chem. Geol.* 577, 120294. <https://doi.org/10.1016/j.chemgeo.2021.120294>.

- Heilbron, M., Valeriano, C.D.M., Valladares, C.S., Machado, N., 1995. A orogênese brasileira no segmento central da Faixa Ribeira, Brasil. *Braz. J. Geol.* 25, 249–266. <https://doi.org/10.25249/0375-7536.1996249266>.
- Heilbron, M., Mohriak, W., Valeriano, C.M., Milani, E., Almeida, J.C.H., Tupinambá, M., 2000. From collision to extension: The roots of the southeastern continental margin of Brazil. In: Talwani, M., Mohriak, W. (Eds.), *Atlantic Rifts and Continental Margins*, vol. 115. American Geophysical Union, Washington, DC, pp. 1–34. <https://doi.org/10.1029/GM115p0001>. Geophysical Monograph Series.
- Heilbron, M., Valeriano, C.D.M., Tassinari, C.C.G., Almeida, J., Tupinamba, M., Siga Jr., O., Trouw, R., 2008. Correlation of Neoproterozoic terranes between the Ribeira Belt, SE Brazil and its African counterpart: comparative tectonic evolution and open questions. *Geol. Soc. Lond. Spec. Publ.* 294, 211–237. <https://doi.org/10.1144/SP294.12>.
- Heilbron, M., Ribeiro, A., Valeriano, C.M., Paciullo, F.V., Almeida, J.C.H., Trouw, R.J.A., Tupinambá, M., Eirado Silva, L.G., 2017. The Ribeira Belt. In: Heilbron, M., Cordani, U.G., Alkmim, F.F. (Eds.), *São Francisco Craton, Eastern Brazil: Tectonic Genealogy of a Miniature Continent*. Springer Nature, Switzerland, pp. 277–302. <https://doi.org/10.1007/978-3-319-01715-0>.
- Hilton, D.R., 1996. The helium and carbon isotope systematics of a continental geothermal system: results from monitoring studies at Long Valley caldera (California, USA). *Chem. Geol.* 127, 269–295. [https://doi.org/10.1016/0009-2541\(95\)00134-4](https://doi.org/10.1016/0009-2541(95)00134-4).
- Italiano, F., Yuce, G., Uysal, I.T., Gasparon, M., Morelli, G., 2014. Insights into mantle-type volatiles contribution from dissolved gases in artesian waters of the Great Artesian Basin, Australia. *Chem. Geol.* 378, 75–88. <https://doi.org/10.1016/j.chemgeo.2014.04.013>.
- Ju, Y., Gilfillan, S.M., Lee, S.S., Kaown, D., Hahm, D., Lee, S., Park, I.W., Ha, S.S., Park, K., Do, H.K., Yun, S.T., Lee, K.K., 2020. Application of noble gas tracers to identify the retention mechanisms of CO<sub>2</sub> migrated from a deep reservoir into shallow groundwater. *Int. J. Greenhouse Gas Control* 97, 103041. <https://doi.org/10.1016/j.ijgge.2020.103041>.
- Karlstrom, K.E., Crossey, L.J., Hilton, D.R., Barry, P.H., 2013. Mantle <sup>3</sup>He and CO<sub>2</sub> degassing in carbonic and geothermal springs of Colorado and implications for neotectonics of the Rocky Mountains. *Geology* 41, 495–498. <https://doi.org/10.1130/G34007.1>.
- Karolyte, R., Johnson, G., Györe, D., Serno, S., Flude, S., Stuart, F.M., Chivas, A.R., Boyce, A., Gilfillan, S.M., 2019. Tracing the migration of mantle CO<sub>2</sub> in gas fields and mineral water springs in south-East Australia using noble gas and stable isotopes. *Geochim. Cosmochim. Acta* 259, 109–128. <https://doi.org/10.1016/j.gca.2019.06.002>.
- Kennedy, B.M., Van Soest, M.C., 2007. Flow of mantle fluids through the ductile lower crust: helium isotope trends. *Science* 318 (5855), 1433–1436. <https://doi.org/10.1126/science.1147537>.
- Kerrick, D.M., 2001. Present and past nonanthropogenic CO<sub>2</sub> degassing from the solid Earth. *Rev. Geophys.* 39 (4), 565–585. <https://doi.org/10.1029/2001RG000105>.
- Kipfer, R., Aeschbach-Hertig, W., Peeters, F., Stute, M., 2002. Noble gases in lakes and ground waters. In: Porcelli, D., Ballentine, C.J., Wieler, R. (Eds.), *Noble Gases in Geochemistry and Cosmochemistry*, Washington D. C., Min. Soc. Of Am., 47, pp. 615–700. <https://doi.org/10.2138/rmg.2002.47.14>.
- Klemperer, S.L., Kennedy, B.M., Sastry, S.R., Makovsky, Y., Harinarayana, T., Leech, M. L., 2013. Mantle fluids in the Karakoram fault: Helium isotope evidence. *Earth Planet. Sci. Lett.* 366, 59–70. <https://doi.org/10.1016/j.epsl.2013.01.013>.
- Klemperer, S.L., Zhao, P., Whyte, C.J., Darrah, T.H., Crossey, L.J., Karlstrom, K.E., Ding, L., 2022. Limited underthrusting of India below Tibet: 3He/4He analysis of thermal springs locates the mantle suture in continental collision. *Proc. Natl. Acad. Sci.* 119 (12), e2113877119. <https://doi.org/10.1073/pnas.2113877119>.
- LaForce, T., Ennis-King, J., Boreham, C., Paterson, L., 2014. Residual CO<sub>2</sub> saturation estimate using noble gas tracers in a single-well field test: the CO2CRC Otway project. *Int. J. Greenhouse Gas Control* 26, 9–21. <https://doi.org/10.1016/j.ijgge.2014.04.009>.
- Lange, T.P., Palcsu, L., Szakács, A., Kővágó, Á., Gelencsér, O., Gál, Á., Gyila, S., Tóth, T. M., Matenco, L., Krézsek, Cs., Lenkey, L., Szabó, Cs., Kovács, I.J., 2023. The link between lithospheric scale deformations and deep fluid emanations: Inferences from the Southeastern Carpathians. *Evolving Earth, Romania*. <https://doi.org/10.1016/j.eve.2023.100013>.
- Li, M., Wang, T., Liu, J., Lu, H., Wu, W., Gao, L., 2008. Occurrence and origin of carbon dioxide in the Fushan Depression, Beibuwan Basin, South China Sea. *Mar. Pet. Geol.* 25, 500–513. <https://doi.org/10.1016/j.marpetgeo.2007.07.007>.
- Mächler, L., Peter, S., Brennwald, M.S., Kipfer, R., 2013. Excess air formation as a mechanism for delivering oxygen to groundwater. *Water Resour. Res.* 49, 6847–6856. <https://doi.org/10.1002/wrcr.20547>.
- Mantovani, M.S.M., Quintas, M.C.L., Shukowsky, W., Brito Neves, B., 2005. Delimitation of the Paranapanema Proterozoic block: a geophysical contribution. *Episodes J. Int. Geosci.* 28, 18–22. <https://doi.org/10.18814/epiugs/2005/v28i1/002>.
- Marques, J.M., Carreira, P.M., Aires-Barros, L., Graça, R.C., 2000. Nature and role of CO<sub>2</sub> in some hot and cold HCO<sub>3</sub><sup>-</sup>/Na<sup>+</sup>/CO<sub>2</sub>-rich Portuguese mineral waters: a review and reinterpretation. *Environ. Geol.* 40, 53–63. <https://doi.org/10.1007/s002540000151>.
- Marty, B., Jambon, A., 1987. C<sub>3</sub>He in volatile fluxes from the solid Earth: implications for carbon geodynamics. *Earth Planet. Sci. Lett.* 83 (1–4), 16–26. [https://doi.org/10.1016/0012-821X\(87\)90047-1](https://doi.org/10.1016/0012-821X(87)90047-1).
- Marty, B., Tolstikhin, I.N., 1998. CO<sub>2</sub> fluxes from mid-ocean ridges, arcs and plumes. *Chem. Geol.* 145 (3–4), 233–248. [https://doi.org/10.1016/S0009-2541\(97\)00145-9](https://doi.org/10.1016/S0009-2541(97)00145-9).
- Marty, B., Zimmermann, L., 1999. Volatiles (He, C, N, Ar) in mid-ocean ridge basalts: Assesment of shallow-level fractionation and characterization of source composition. *Geochim. Cosmochim. Acta* 63 (21), 3619–3633. [https://doi.org/10.1016/S0016-7037\(99\)00169-6](https://doi.org/10.1016/S0016-7037(99)00169-6).
- Meert, J.G., Van Der Voo, R., 1997. The assembly of gondwana 800–550 Ma. *J. Geodyn.* 23 (3–4), 223–235.
- Meisling, K.E., Cobbold, P.R., Mount, V.S., 2001. Segmentation of an obliquely rifted margin, Campos and Santos basins, southeastern Brazil. *AAPG Bull.* 85, 1903–1924. <https://doi.org/10.1306/8626D0A9-173B-11D7-8645000102C1865D>.
- Meneghini, A.A., Wakasugi, D.S.M., Santos, A.B. dos, Damatto, S.R., Salvador, V.L.R., 2019. Inorganic chemical elements determined in mineral water springs from the water circuit of Minas Gerais, Brazil by X-ray fluorescence spectrometry. In: *Internacional Atlantic Conference - INAC 2019, Santos, SP (Anais International Nuclear Atlantic Conference 2019, 529-540)*.
- Morrison, P., Pine, J., 1955. Radiogenic origin of the helium isotopes in rock. *Ann. N. Y. Acad. Sci.* 62, 71–92. <https://doi.org/10.1111/j.1749-6632.1955.tb35366.x>.
- Paciullo, F.V.P., Ribeiro, A., Andreis, R.R., Trouw, R.A.J., 2000. The Andrelândia basin, a neoproterozoic intraplate continental margin, southern Brasília Belt, Brazil. *Revista Brasileira de Geociências* 30, 200–202. <https://doi.org/10.25249/0375-7536.2000301200202>.
- Pinti, D.L., Marty, B., 1998. The origin of helium in deep sedimentary aquifers and the problem of dating very old groundwaters. *Geol. Soc. Lond. Spec. Publ.* 144 (1), 53–68. <https://doi.org/10.1144/GSL.SP.1998.144.01.05>.
- Ribeiro, A., Teixeira, W., Dussin, I.A., Ávila, C.A., Nascimento, D., 2013. U-Pb LA-ICP-MS detrital zircon ages of the São João do Rei and Carandaí basins: new evidence of intermittent Proterozoic rifting in the São Francisco paleocontinent. *Gondwana Res.* 24, 713–726. <https://doi.org/10.1016/j.gr.2012.12.016>.
- Riccomini, C., Velázquez, V.F., Gomes, C.B., 2005. Tectonic controls of the Mesozoic and Cenozoic alkaline magmatism in central-southeastern Brazilian Platform. In: *Mesozoic to Cenozoic alkaline magmatism in the Brazilian Platform*, 123, pp. 31–56. Available at: <https://repositorio.usp.br/bitstreams/3a4d3632-b844-4fa2-b727-d5be5fd41580#page=27>.
- Ring, U., Uysal, I.T., Yüce, G., Ünal-İmer, E., Italiano, F., İmer, A., Zhao, J.X., 2016. Recent mantle degassing recorded by carbonic spring deposits along sinistral strike-slip faults, south-Central Australia. *Earth Planet. Sci. Lett.* 454, 304–318. <https://doi.org/10.1016/j.epsl.2016.09.017>.
- Ros, E., Pérez-Gussinyé, M., Araújo, M., Thoaldo, R.M., Andrés-Martínez, M., Morgan, J. P., 2017. Lower crustal strength controls on melting and serpentinization at magma-poor margins: potential implications for the South Atlantic. *Geochem. Geophys. Geosyst.* 18, 4538–4557. <https://doi.org/10.1002/2017GC007212>.
- Sano, Y., Marty, B., 1995. Origin of carbon in fumarolic gas from island arcs. *Chem. Geol.* 119, 265–274. [https://doi.org/10.1016/0009-2541\(94\)00097-R](https://doi.org/10.1016/0009-2541(94)00097-R).
- Santos, L.A.B., Damatto, S.R., 2017. Determination of the <sup>226</sup>Ra, <sup>228</sup>Ra and <sup>210</sup>Pb concentrations in the mineral water springs from Water Parks of Cambuquira and Marimbeiro, Minas Gerais and Assessment of the Committed Effective Doses. In: *International Nuclear Atlantic Conference INAC 2017, Belo Horizonte*.
- Sial, A.N., Ferreira, V.P., De Almeida, A.R., Romano, A.W., Parente, C.V., Da Costa, M.L., Santos, V.H., 2000. Carbon isotope fluctuations in Precambrian carbonate sequences of several localities in Brazil. *An. Acad. Bras. Ciênc.* 72, 539–558. <https://doi.org/10.1590/S0001-37652000000400006>.
- Torgersen, T., Clarke, W.B., 1985. Helium accumulation in groundwater, I: an evaluation of sources and the continental flux of crustal <sup>4</sup>He in the Great Artesian Basin, Australia. *Geochim. Cosmochim. Acta* 49, 2445–2454. [https://doi.org/10.1016/0016-7037\(85\)90011-0](https://doi.org/10.1016/0016-7037(85)90011-0).
- Trouw, C.C., de Medeiros, F.F.F., Trouw, R.A.J., 2008. Evolução tectônica da Zona de Cisalhamento Caxambu, MG. *Braz. J. Geol.* 37, 767–776. <https://doi.org/10.25249/0375-7536.2007374767776>.
- Trouw, R.A., Peternel, R., Ribeiro, A., Heilbron, M., Vinagre, R., Duffles, P., Trouw, C.C., Fontainha, M., Kussama, H.H., 2013. A new interpretation for the interference zone between the southern Brasília belt and the Central Ribeira belt, SE Brazil. *J. S. Am. Earth Sci.* 48, 43–57. <https://doi.org/10.1016/j.james.2013.07.012>.
- Trouw, R.A.J., Paciullo, F.V.P., Ribeiro, A., 1994. A Faixa Alto Rio Grande reinterpretada como zona de interferência entre a Faixa Brasília e a Faixa Ribeira. *SBG, Congresso Bras. Geologia* 38, 234–235.
- Trouw, R.A.J., Heilbron, M., Ribeiro, A., Paciullo, F.V.P., Valeriano, C.M., Almeida, J.C. H., Tupinambá, M., Andreis, R.R., 2000. The Central Segment of the Ribeira Belt. In: Cordani, U.G., Milani, E.J., Thomaz Filho, A., Campos, D.A. (Eds.), *Tectonic evolution of South America, Rio de Janeiro 31st International Geological Congress*, pp. 287–310.
- Trouw, R.A.J., Peternel, R., Medeiros, F.F.F., Trouw, C.C., Rodrigues, L.H.O., 2003. The Neoproterozoic Caxambu Shear Zone, MG. *SBG. Simp. Nac. Estudos Tectônicos* 9, 124–127.
- Ulbrich, H.H.G., Gomes, C.D.B., 1981. Alkaline rocks from continental Brazil. *Earth Sci. Rev.* 17 (1–2), 135–154.
- Umeda, K., Ninomiya, A., 2009. Helium isotopes as a tool for detecting concealed active faults. *Geochem. Geophys. Geosyst.* 10. <https://doi.org/10.1029/2009GC002501>.
- Valeriano, C.D.M., Pimentel, M.M., Heilbron, M., Almeida, J.C.H., Trouw, R.A.J., 2008. Tectonic evolution of the Brasília Belt, Central Brazil, and early assembly of Gondwana. *Geol. Soc. Lond. Spec. Publ.* 294, 197–210. <https://doi.org/10.1144/SP294.11>.
- Valeriano, C.M., 2017. The Southern Brasília Belt. In: Heilbron, M., Cordani, U.G., Alkmim, F.F. (Eds.), *São Francisco Craton*. Springer, Eastern Brazil, pp. 189–203. <https://doi.org/10.1007/978-3-319-01775-0>.
- Valeriano, C.M., Machado, N., Simonetti, A., Valladares, C.S., Seer, H.J., Simões, L.S., 2004. U-Pb Geochronology of the southern Brasília Belt (SE Brazil): sedimentary provenance, Neoproterozoic orogeny and assembly of WestGondwana. *Precambrian Res.* 130, 27–55. <https://doi.org/10.1016/j.precamres.2003.10.014>.

- Weiss, R., 1974. Carbon dioxide in water and seawater: the solubility of a non-ideal gas. *Mar. Chem.* 2 (3), 203–215. [https://doi.org/10.1016/0304-4203\(74\)90015-2](https://doi.org/10.1016/0304-4203(74)90015-2).
- Weiss, R.F., 1970. The solubility of nitrogen, oxygen and argon in water and seawater. *Deep-Sea Res. Oceanogr. Abstr.* 17, 721–735. [https://doi.org/10.1016/0011-7471\(70\)90037-9](https://doi.org/10.1016/0011-7471(70)90037-9).
- Werner, C., Brantley, S., 2003. CO<sub>2</sub> emissions from the Yellowstone volcanic system. *Geochem. Geophys. Geosyst.* 4 (7). <https://doi.org/10.1029/2002GC000473>.
- Yasin, D., Yüce, G., 2023. Isotope and hydrochemical characteristics of thermal waters along the active fault zone (Erzin-Hatay/Turkey) and their geothermal potential. *Turk. J. Earth Sci.* 32 (6), 721–739. <https://doi.org/10.55730/1300-0985.1871>.
- Zalán, P.V., Severino, M.D.C.G., Rigoti, C.A., Magnavita, L.P., Oliveira, J.A.B., Viana, A.R., 2011. An entirely new 3D-view of the crustal and mantle structure of a South Atlantic passive margin—Santos, Campos and Espírito Santo basins, Brazil. In: AAPG annual conference and Exhibition, Texas, USA, Expanded Abstract, 1–12, Article 30177.
- Zappone, A., Rinaldi, A.P., Grab, M., Wenning, Q.C., Roques, C., Madonna, C., Obermann, A.C., Bernasconi, S.M., Brennwald, M.S., Kipfer, R., Soom, F., Cook, P., Guglielmi, Y., Nussbaum, C., Giardini, D., Mazzotti, M., Wiemer, S., 2021. Fault sealing and caprock integrity for CO<sub>2</sub> storage: an in situ injection experiment. *Solid Earth* 12, 319–343. <https://doi.org/10.5194/se-12-319-2021>.
- Zhang, M., Guo, Z., Xu, S., Barry, P.H., Sano, Y., Zhang, L., Li, Y., 2021. Linking deeply-sourced volatile emissions to plateau growth dynamics in southeastern Tibetan Plateau. *Nat. Commun.* 12 (1), 4157. <https://doi.org/10.1038/s41467-021-24415-y>.